# Using Computational Chemistry to Reveal Nature's Blueprints for Single-Site Catalysis of C–H Activation

Aditya Nandy[1,2], Husain Adamji[1], David W. Kastner[1,3], Vyshnavi Vennelakanti[1,2], Azadeh Nazemi[1], Mingjie Liu[1], and Heather J. Kulik[1,*]

[1]*Department of Chemical Engineering, Massachusetts Institute of Technology, Cambridge, MA 02139, USA*

[2]*Department of Chemistry, Massachusetts Institute of Technology, Cambridge, MA 02139, USA*

[3]*Department of Biological Engineering, Massachusetts Institute of Technology, Cambridge, MA 02139, USA*

ABSTRACT: The challenge of activating inert C–H bonds motivates a study of catalysts that draws from what can be accomplished by natural enzymes and translates these advantageous features into transition-metal complex (TMC) and material mimics. Inert C–H bond activation reactivity has been observed in a diverse number of predominantly iron-containing enzymes from the heme-P450s to non-heme iron α-ketoglutarate-dependent enzymes and methane monooxygenases. Computational studies have played a key role in correlating active site variables such as the primary coordination sphere, oxidation state, and spin state to reactivity. TMCs, zeolites, metal organic frameworks (MOFs), and single-atom catalysts (SACs) are synthetic inorganic materials that have been designed to incorporate Fe active sites in analogy to single sites in enzymes. In these systems, computational studies have been essential in supporting spectroscopic assignments and quantifying the effects of the metal-local environment on C–H bond reactivity. High-throughput virtual screening tools that have been widely used for bulk metal catalysis do not readily extend to the single-site inorganic catalysts where metal–ligand bonding and localized *d*-electrons govern reaction energetics. These localized *d*-electrons can also necessitate wavefunction theory calculations when density functional theory (DFT) is not sufficiently accurate. Where sufficient computational or experimental data can be gathered, machine learning has helped uncover more general design rules for reactivity or stability. As we continue to investigate metalloprotein active sites, we gain insights that enable us to design stable, active, and selective single-site catalysts.

Keywords: C–H activation, QM/MM, enzyme catalysis, metal-oxo species, density functional theory, bioinspired catalyst design

## 1. Introduction.

Selective partial C–H bond activation remains challenging and economically infeasible due to the lack of an industrially effective catalyst that can activate and functionalize inert C–H bonds without overoxidation.[1-2] Metalloenzymes that have mononuclear Fe active sites in high-spin (HS) states[3-5] coordinated to weak-field amino acids can selectively oxidize substrates with inert C–H bonds such as those in light alkanes.[6] Although these metalloenzymes operate at room temperature under mild conditions, they have narrow thermal and pH stability windows. Hence, they are not practical for industrial-scale C–H bond activation and functionalization.[6] Nonetheless, the identification of metal-oxo moieties within metalloenzyme active sites that are thought to be potent oxidants in C–H activation have led to many spectroscopic[7-9] and computational[8-9] studies to uncover the role of this elusive intermediate.

The metal-oxo moieties present in metalloenzymes that can activate inert C–H bonds are challenging to isolate or characterize[10] but have inspired the design of Fe-containing transition-metal complexes (TMCs) that contain metal-oxo bonds.[11-13] Although metal-oxo moieties in TMCs are easier to isolate and characterize by crystallography[14] and spectroscopy[14-16] than those in a biological context, they also remain elusive and challenging to study. Computational studies[17-18] play an essential role in understanding these Fe metal-oxo intermediates and their electronic structure to elucidate C–H bond activation mechanisms[19] and draw comparisons to metalloenzymes.[20] In particular, the active sites of metalloenzymes have motivated the synthesis of bioinspired TMCs to quantify reactivity trends.[21-22]

Single-site heterogeneous catalysts represent one way to overcome potential limitations of industrial application of TMCs or enzymes. Zeolites, MOFs, and SACs are promising materials for practical use because they can be more readily separated from products and

reactants. The active sites in metalloenzymes have inspired incorporation of isolated Fe atoms in these materials that can also carry out C–H bond activation.[23-24] The complex nature of these systems and challenges of achieving atomic precision with spectroscopic techniques has required a tight interplay between characterization and simulation. Nevertheless, further developments are needed both in increasing the computational speed (e.g., with machine learning) and accuracy (e.g., by going beyond DFT) to enable rapid discovery and design.

In this Perspective, we highlight the role of computational studies in understanding C–H bond activation in metalloenzymes, TMCs, and single-site heterogeneous catalysts such as zeolites, MOFs, and SACs (Figure 1). We first highlight studies on metalloenzyme C–H bond reactivity and the role of computational studies in confirming spectroscopic observations and uncovering mechanisms. We then discuss how these metalloenzyme active sites have inspired the design of TMCs, zeolites, MOFs, and SACs. In each subclass of materials, we illustrate the unique role of computational studies in providing insights into C–H bond activation. In particular, we underscore the importance of computational studies in unraveling the role of spin state and active site environment on C–H bond reactivity, both of which are challenging to probe by experiment. Lastly, we call attention to tools and techniques that bridge analysis of C–H bond reactivity across different systems and emphasize the role of machine learning (ML) for future bioinspired materials design.

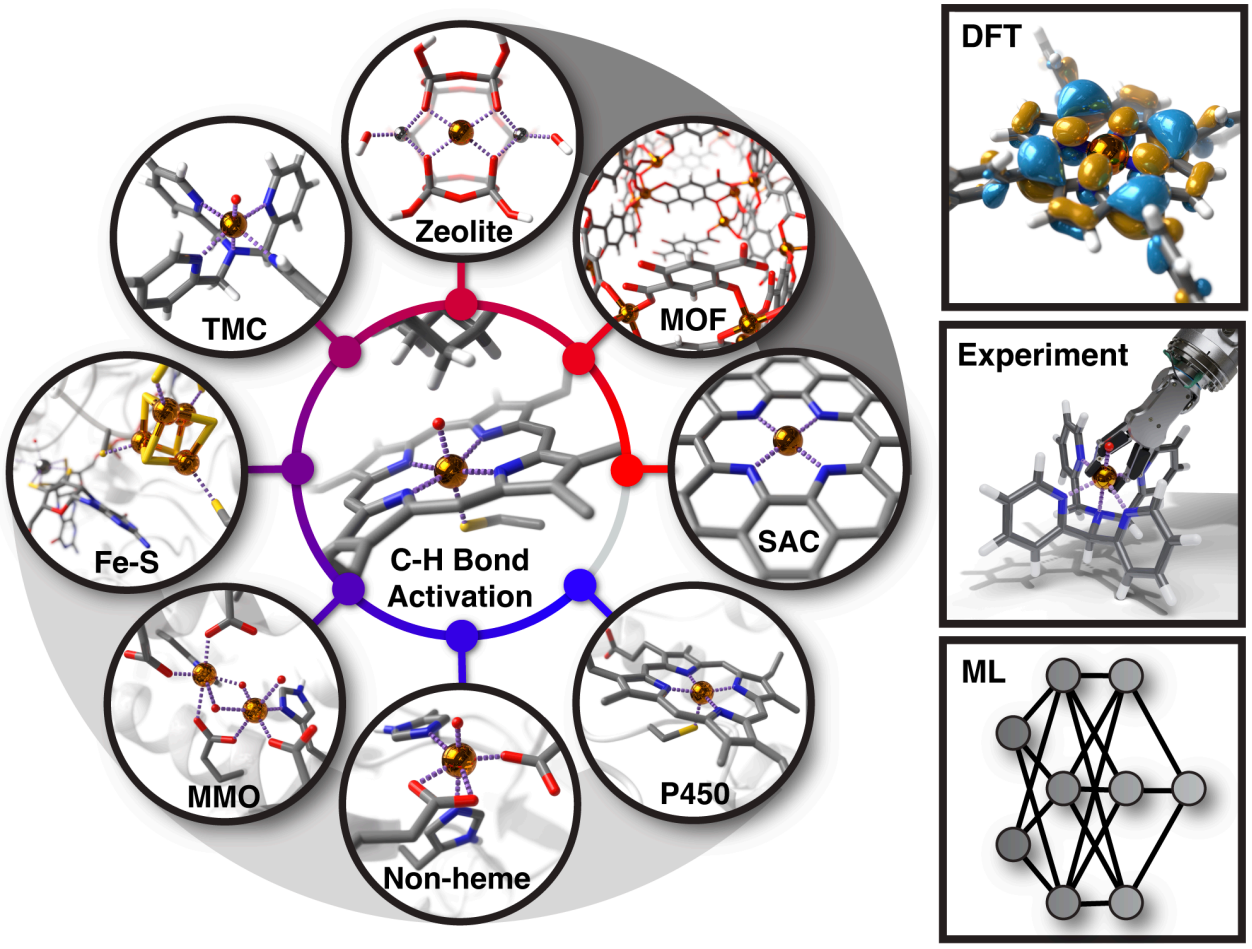


**Figure 1.** An illustrative overview of iron-containing systems studied for catalytic C–H activation. The scope covers three domains of catalysis: enzymes (light gray band), transition-metal complexes, and heterogenous single-site catalysts (dark gray band). The range of studied systems and their depicted structures include cytochrome P450 enzymes (PDB: 5CP4), non-heme iron α-ketoglutarate-dependent oxygenases (PDB: 1OS7), methane monooxygenases(MMO, PDB: 1MTY), FeS cluster cofactor-containing enzymes (PDB: 1FDO), zeolites (Fe-ZSM-5), metal-organic frameworks (MOFs, Fe-MOF-74), and single-atom catalysts (SACs, $FeN_4$ embedded in graphene). Systems are explored using density functional theory (DFT), experiments, and machine learning (ML).

*2. Metalloenzymes That Catalyze C–H Bond Activation*

Metalloenzymes readily activate and functionalize inert C–H bonds of various substrates at isolated Fe, Cu, and Mo metal centers. A diverse number of Fe-containing metalloenzymes have the ability to activate C–H bonds: heme-P450, non-heme α-ketoglutarate-dependent enzymes, soluble methane-monooxygenase enzymes, and Fe-S-cluster-dependent

metalloenzymes. All of these enzymes utilize Fe at some point in the process of C–H bond activation. Computational studies have played a key role in confirming spectroscopic assignments that provide proof of fleeting reactive intermediates that are essential for drawing conclusions about the chemical mechanism. Additionally, these studies have also uncovered the role of various active site variables such as coordination environment, noncovalent interactions, and substrate positioning that pave the way for bioinspired catalyst design.

*2.1 Heme-P450 Enzymes*

Heme-containing P450 enzymes were the first enzymes studied for selective C–H bond hydroxylation.[25-26] A reactive metal-oxo intermediate was identified by Mössbauer spectroscopy and hypothesized as the reactive species in chloroperoxidase[27] but could not be crystallographically characterized. Due to the similarity of reactivity signatures obtained from isotope labeling studies (i.e., kinetic isotope effects) between the chloroperoxidase and P450s, the metal-oxo intermediate was hypothesized to be the active species in P450s but was fleeting and difficult to trap.[26] Groves and McCluskey utilized isotope labeling studies on model ferrous ion-peroxyacid systems and discovered the radical rebound mechanism, which is now the predominant proposed mechanism for C–H hydroxylation[25, 28-29] (Figure 2). This name of this mechanism for alcohol formation refers to the "rebound" of a substrate-centered carbon radical with the post-C–H activation metal-hydroxo moiety formed by the metal-oxo subunit.[25] Despite the elucidation of the radical rebound mechanism, trends in P450 reactivity, such as product selectivity (e.g. the distribution between hydroxylation vs. epoxidation products), remained difficult to explain.[30-31] To explain these trends, Shaik and coworkers used DFT and developed the concept of multistate reactivity[32-33], in which the spin state changes along a reaction coordinate. In particular, a mechanism invoking two-state reactivity (TSR) with differences in

reactivity on the triplet and quintet spin state surfaces could explain why both epoxidation and hydroxylation products formed, emphasizing the role of spin in P450 reactivity.[34-35]

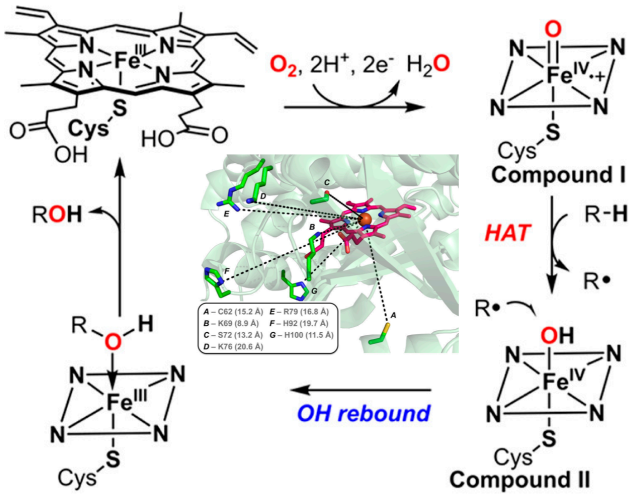


**Figure 2.** The radical rebound mechanism for C–H bond hydroxylation as performed by heme-P450 enzymes at Fe centers. Catalytic cycle adapted with permission from ref. 29. Copyright 2017 American Chemical Society. P450 enzyme active site adapted with permission from ref. 31. Copyright 2016 American Chemical Society.

DFT was also essential in understanding the environmental factors that influence reactivity at the P450 metal-oxo active site. Ogliaro *et al*. investigated the role of polarizability in the axial cysteine ligation to heme and found that hydrogen bond donors adjacent to the metal–sulfur bond affect its bond length and coordination strength, highlighting the influence of the greater protein environment and hydrogen bonding on reactivity.[36] A multi-scale quantum mechanics/molecular mechanics (QM/MM) study by Guallar *et al.* determined that peripheral carboxylate substituents on the heme co-factor stabilize nearby charged residues and influence hydrogen atom abstraction reactivity by promoting charged interactions in the transition state (TS).[37] Computational studies also shed light on long-range effects in P450s that cannot easily be understood with experiment alone. A recent computational study by Acevedo-Rocha *et al*. found that a single amino-acid substitution induces long-range conformational changes that alter gating mechanisms and thus hydroxylation selectivity, providing future opportunities to engineer

P450s.[38] More recently, Bím *et al*. found that axial ligation induces large local electric fields in P450s and other heme-containing enzymes (e.g. catalases and peroxidases). Using DFT calculations, they found that the axial cysteine ligation induces the strongest electric field, which enables P450s to uniquely undergo hydrogen atom transfer (HAT) from strong C–H bonds in light alkanes.[39]

Although P450 heme enzymes catalyze challenging oxygenation reactions, they do not possess native carbene transfer reactivity. Coelho *et al*. used directed evolution to extend metal-oxo reactivity to isoelectronic metal-carbene transfer reactivity.[40] Recently, Dodani *et al*. used molecular dynamics to guide selection of a single amino-acid substitution that alters the conformational substrate gating of a P450 enzyme and experimentally changed nitration regioselectivity on a L-tryptophan substrate.[41] While directed evolution proves that P450 reactivity and regioselectivity can be engineered, simulation plays a pivotal role in dissecting the mechanisms by which incorporated substitutions alter substrate and reaction selectivity.

*2.2 Non-Heme Fe α-Ketoglutarate-Dependent Hydroxylase and Halogenase Enzymes*

Since the discovery of the first Fe(II)/α-ketoglutarate-dependent mononuclear oxygenases, the study of this non-heme iron family of enzymes has revealed a wealth of substrate and reaction diversity essential to biology.[42] The Fe(II)/α-ketoglutarate-dependent oxygenase family displays a range of catalytic mechanisms despite a conserved coordination environment, with many of the members containing a HS Fe(II) center.[7, 43] The active site of hydroxylases, a subset of the oxygenase superfamily, contains a conserved 2-His-1-carboxylate facial triad and HS Fe(II) center within a conserved double-stranded β-helix fold.[7] In halogenases, the coordinating facial triad carboxylate is substituted for an alanine or glycine, leaving a coordination site for a chloride or bromide ion to bind to iron (Figure 3).[44] Despite

different reactivities, these enzymes share a conserved HAT step for C–H bond activation. During this step, the Fe(IV)-oxo species homolytically cleaves a target substrate C–H bond, yielding a radical intermediate.[45] For the hydroxylase class of Fe(II)/α-ketoglutarate-dependent enzymes, the radical intermediate then recombines with the Fe(III)-hydroxo moiety, generating the hydroxylated product as part of the radical rebound step, as first observed in the P450 family of enzymes. Characterization of the HS state in the archetypal enzyme TauD by Bollinger and Krebs has informed synthetic efforts to design HS molecular mimics.[13-14, 44] Although the Fe(II)-coordinating residue identities are essential for catalytic activity, computational investigations of Fe(II)/α-ketoglutarate-dependent oxygenases reveal that reaction selectivity extends beyond the immediate coordinating environment and incorporates aspects of binding pocket interactions, substrate positioning, and local electric fields.[46-49]

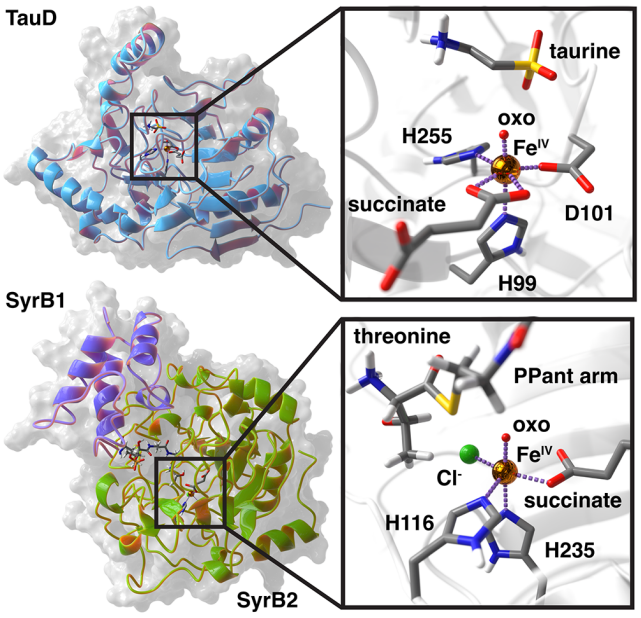


**Figure 3.** Structures and active sites of TauD and the SyrB2-SyrB1 complex. (top) The structure of the hydroxylase TauD (blue). The active site is highlighted with an inset and contains an Fe(IV)-oxo, succinate, and three coordinating residues labeled with their one-letter codes (H99, D101, and H255). Coordinates for the resting state of the were obtained from the PDB (PDB ID: 6EDH), and the oxo and succinate were modeled into these structures and hydrogen atoms were added. (bottom) The structure of the halogenases SyrB1 (purple) and SyrB2 (green). The active site is highlighted with an inset and contains an Fe(IV)-oxo, succinate, a chloride, and two

coordinating residues labeled with their one-letter codes (H116, H235). Coordinates were obtained from ref. 47 in which SyrB2 was obtained from the PDB (PDB ID: 2FCT), the oxo and succinate were modeled into these structures, and hydrogen atoms were added. Additionally, a homology model of SyrB1 was generated in ref. 47 and docked into the structure of SyrB2.

The array of chemical transformations performed by Fe(II)/α-ketoglutarate-dependent oxygenases span hydroxylation[7], halogenation[50], desaturation[43], carbon–carbon cleavage[51], and more recently, isonitrile formation[52-53], with some multi-functional non-heme iron enzymes able to perform different reactions under different conditions.[54-55] For the well-studied halogenase SyrB2, experimental and computational investigations have revealed that the position of the substrate correlates to whether rebound of the chloride or hydroxyl is observed.[56-57] A more complete understanding of the factors governing the relative propensity toward halogenation or hydroxylation is an important prerequisite for the design of novel halogenases and synthetic mimics capable of halogenation.[58] Computational studies suggest that SyrB1, the carrier protein that works with SyrB2, plays an essential role in halogenation selectivity by positioning the substrate deeper into the active site where the substrate forms cooperative hydrogen bonds with the secondary coordinating residue Asn123 (Figure 3).[47, 49] In addition, the second-sphere residue Arg254 has been proposed to play a mechanistic role in active site isomerization and inhibition of hydroxyl rebound, favoring radical recombination of the halide.[59-60] In contrast to SyrB1/SyrB2, BesD and WelO5 are both halogenases that do not require carrier proteins. Instead, BesD positions its substrate through multiple hydrogen bonds and charged interactions, while WelO5 relies on hydrophobic interactions and active site isomerization.[61-63]

For ScoE, a recently discovered isonitrile-forming enzyme, many mechanisms were proposed prior to crystallographic characterization of the protein–substrate conformation. These mechanisms ranged from hydroxylation to desaturation and nitrogen activation.[64-66] Recent

computational and experimental studies based on the crystal structure, however, have shed light on the mechanism, revealing key hydrogen bonding interactions between the substrate and the protein environment that orient the substrate[52-53] (Figure 4). This precise substrate orientation facilitates C5–H abstraction rather than at the weaker proximal N–H bond. This C5–H bond activation and the subsequent hydroxyl rebound step align with an experimentally observed on-pathway hydroxylated intermediate.[52-53]

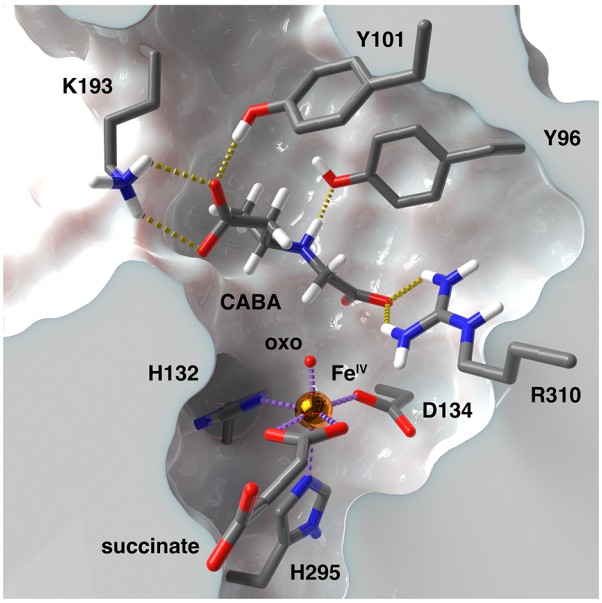


**Figure 4.** The active site of the isonitrile-forming enzyme ScoE. Key hydrogen bonding interactions involved in orienting the substrate are shown as yellow dashed bonds between the substrate CABA and the residues labeled with their one-letter codes (Y96, Y101, K193, R310).

Many recent computational studies have focused on determining the role of noncovalent interactions (NCIs) originating from the secondary coordination sphere on reactivity and selectivity.[46, 48] The role of the secondary coordination sphere is particularly evident when comparing different Fe(II)/α-ketoglutarate-dependent oxygenases that act on the same substrate. The enzymes VioC, OrfP, EFE, and NapI all act on L-arginine, but carry out distinct oxidative transformations.[54, 67-70] The L-arginine substrate contains three aliphatic carbons, each a potential

target for C–H activation.[71] Recent computational studies have thus focused on understanding what distinguishes these enzymes despite sharing identical substrates.[46, 48] For VioC, quantum mechanical (QM) cluster model calculations found that local electric fields dramatically increase the favorability of the C3–H abstraction while disfavoring activation of the isoenergetic C4–H bond. Other recent work has found that the unique double hydroxylation activity of OrfP is due to exceptionally strong active-site binding that increases substrate residence time and promotes a second hydroxylation.[68] The distinct reactivity of EFE is believed to be due to a conformational switch that derails the ethylene formation pathway active in other enzymes.[72] Lastly, little is known about the factors that contribute to the C5–H selectivity of NapI and its unique desaturation mechanism. With no computational studies performed to date, NapI illustrates the need for future mechanistic and computational investigation into Fe(II)/α-ketoglutarate-dependent oxygenases to understand the full breadth of reactions possible with this active site.[69]

*2.3 Methane Monooxygenase (MMO) Enzymes*

Methanotrophic bacteria leverage methane monooxygenase (MMO) metalloenzymes to activate the strong C–H bonds in methane and selectively produce methanol under atmospheric conditions using $O_2$ as an oxidant.[73] Intracellular copper levels dictate the expression levels of the form of MMO: soluble MMO (sMMO) genes are expressed under copper-limited conditions, resulting in an iron active site, whereas particulate MMO (pMMO) genes are expressed when copper is abundant, resulting in a copper active site.[74] The structures of sMMO active sites are well-studied compared to those of pMMO.[74] In the case of sMMO, crystallography has revealed that the active site consists of a non-heme di-iron core bridged by exogeneous hydroxides within a hydrophobic cavity[75] (Figure 5).

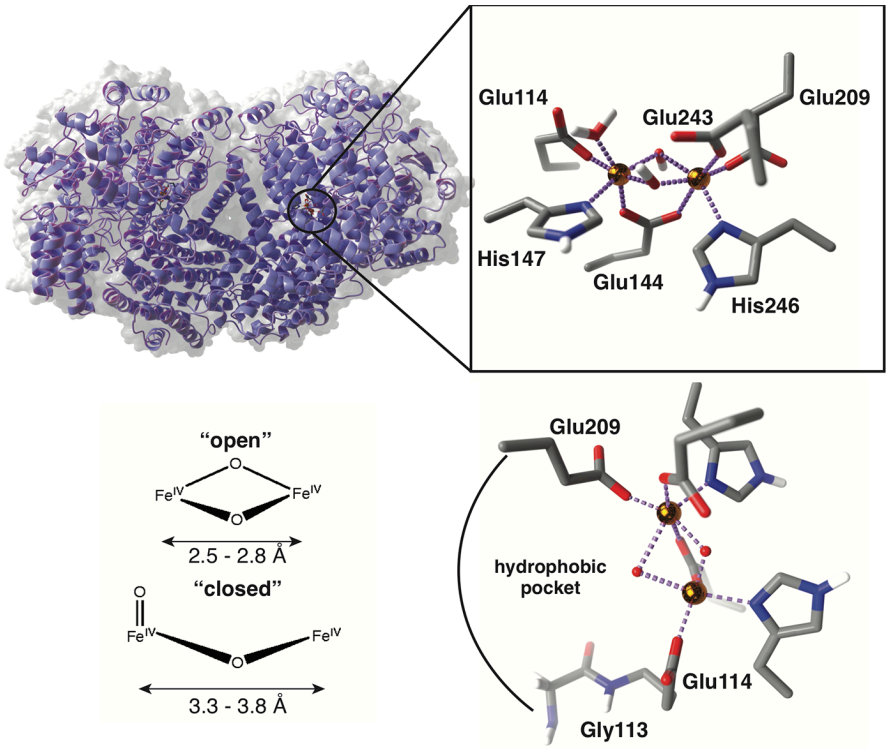


**Figure 5.** (top left) Overall structure of sMMO (PDB: 1MTY) highlighting the location of the di-iron active site. (top right) Enlarged non-heme di-iron active site in sMMO showing the coordinating residues and ligands. (bottom left) Two proposed structures of the Q intermediate essential in light alkane C–H bond activation. (bottom right) Depiction of the hydrophobic substrate binding pocket around the Q intermediate showing the important protein residues involved. Fe atoms are shown in brown, O atoms are shown in red, C atoms are shown in gray, N atoms are shown in blue, and H atoms are shown in white. Di-iron active site structure adapted with permission from ref. 73. Copyright 2011 American Chemical Society. Proposed Q intermediate structures adapted with permission from ref. 76. Copyright 2018 American Chemical Society. Hydrophobic binding site adapted with permission from ref. 77. Copyright 2005 American Chemical Society.

Inspired by P450s, the now widely accepted radical rebound mechanism[25, 28] was suggested for methane hydroxylation by sMMO as well. For sMMO, oxygen insertion into the di-iron site creates the key oxidizing species known as the Q intermediate.[78] The Q intermediate catalyzes HAT from methane followed by methyl radical rebound to form methanol at the active site that is ultimately released.[78] Others have also proposed a non-radical mechanism involving nonsynchronous concerted C–H breaking and C-O forming processes.[79] It is generally agreed that the Q intermediate is the reactive species catalyzing C–H activation, as first observed in

early studies employing transient kinetic techniques coupled with electron paramagnetic resonance (EPR).[80] The structure of the Q intermediate, however, remains heavily debated despite several spectroscopic studies. Thus, computational studies can serve as a valuable tool to understand active site structure and dynamics with atomic precision. For instance, it was first proposed via extended X-ray absorption fine structure (EXAFS) studies that the Q intermediate has a distorted high-valent $Fe_2(\mu\text{–oxo})_2$ diamond core structure where the two iron atoms are antiferromagnetically coupled.[81] More recently however, alternative spectroscopic techniques such as high energy resolution fluorescence-detected X-ray absorption spectroscopy (HERFD XAS) have instead favored an open-core assignment of the Q intermediate, with a terminal Fe(IV)-oxo motif[76, 82] (Figure 5). Hence, these conflicting viewpoints arising from spectroscopic structural assignment of the Q intermediate have motivated researchers to turn to computational studies to gain better insight.

Indeed, QM/MM studies on the Q intermediate that correlate structural motifs to geometric parameters for comparison with experimental EXAFS, Mössbauer, Raman, and HERFD XAS show better agreement with an open-core assignment of the Q intermediate comprising mono-oxo bridged terminal Fe-oxo and Fe-hydroxo species interacting via intramolecular hydrogen bonding.[83] In addition, computational methods are also particularly beneficial in quantifying the role of non-covalent interactions relevant to catalysis, which can be challenging to identify experimentally. Specifically, DFT studies performed on the radical rebound cycle of sMMO highlight the importance of a hydrogen-bonding network surrounding the active site in stabilizing reaction intermediates.[84] Furthermore, QM/MM studies on methane hydroxylation by the Q intermediate explain how methanol selectivity is enhanced. Here, Herman *et al*. argued that the hydrophobic residues in the Q intermediate substrate binding

pocket stabilize the reacting methane through van der Waals interactions and repel the methanol product, triggering its transport away from the active site and preventing overoxidation[77] (Figure 5). These insights gained from MMO have set the stage for bioinspired C–H activation in synthetic homogeneous and heterogeneous catalysts.

*2.4 Fe-S Cluster-Containing Enzymes that Also Depend on Mo/W-Oxos*

Mo/W-containing enzymes activate strong C–H bonds and exhibit hydroxylation reactivity similar to Fe(II)/α-ketoglutarate-dependent oxygenases. One Mo-containing enzyme, ethylbenzene dehydrogenase (EBDH) from the dimethyl sulfoxide (DMSO) reductase family, catalyzes anaerobic hydroxylation of the ethylbenzene to (*S*)-1-phenylethanol.[85] Similar to some Fe(II)/α-ketoglutarate-dependent oxygenases such as VioC, EBDH performs hydroxylation with high stereospecificity.[86] EBDH has a trimeric structure with αβγ subunits[87] (Figure 6). The α-subunit active site includes two molybdopterin guanine dinucleotide ligands, an aspartic acid ligand, and an acetate ligand coordinated to Mo(VI). Together, the coordinating ligands form a distorted trigonal prismatic coordination geometry. A recent bioinspired catalyst design study of formate dehydrogenase (FDH), another Mo/W-containing enzyme in the DMSO reductase family, reported that the enzyme environment primarily affects the geometric properties of the metal center and that these structural variations can improve catalytic properties of the enzyme mimics[88] (Figure 7). While the reactive center contains a Mo/W center and carries out reactions similar to Fe-dependent enzymes, this enzyme family also depends on iron in a distinct modality. The α-subunit contains a [4Fe-4S] cluster is present within 9 Å of one of the molybdopterins in the α-subunit in both FDH and EBDH (Figure 6). The β-subunit is comprised of three [4Fe-4S] and one [3Fe-4S] clusters which all act as redox reservoirs for electrons. The γ-subunit contains a heme *b* cofactor axially ligated by a lysine and methionine to complete the electron transfer

chain of the enzyme.[89-90] Thus, iron plays an important role even when it is not directly binding the substrate.

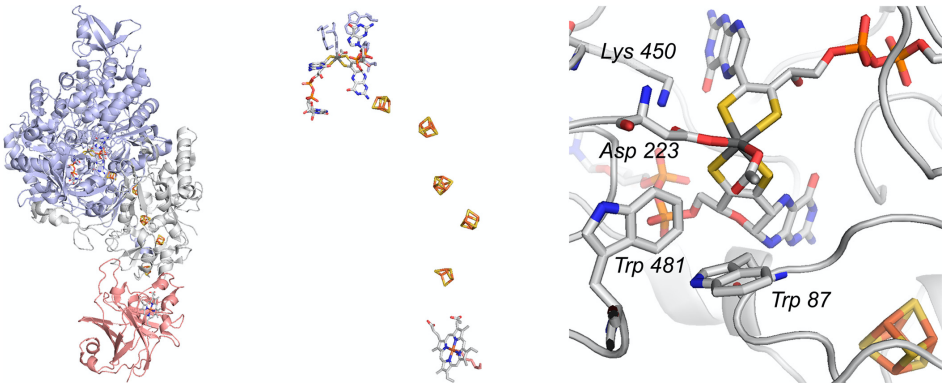


**Figure 6.** Structure of ethylbenzene dehydrogenase from Aromatoleum aromaticum (PDB: 2IVF). (left) The trimeric structure of the enzyme, with the α, β, and γ subunits in blue, gray, and red, respectively. (center) the electron transfer chain of the enzyme, with the molybdenum center at top, iron-sulfur clusters in the middle, and heme at the bottom. (right) the enzyme active site, with the key residues. Reproduced with permission from ref. 87. Copyright 2014 American Chemical Society.

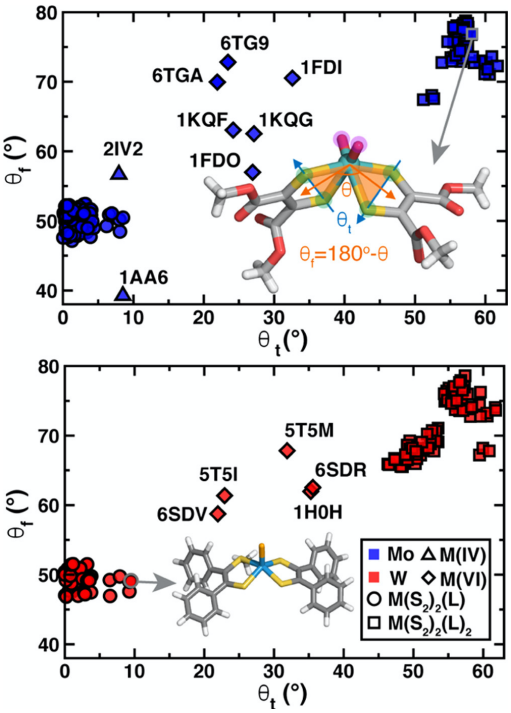


**Figure 7.** Distribution of the twisting ($\theta_t$) and folding ($\theta_f$) angles for Mo (top, blue) and W (bottom, red) complexes containing two dithiolene ligands, relative to FDH enzyme Mo/W cofactors from the PDB labeled by their PDB ID codes. Circles and squares represent five-coordinate and six-coordinate compounds, respectively. In the top panel, an example Mo

compound demonstrates how the twisting and folding angles are defined, with C atoms shown in gray, S in yellow, H in white, O in red, and Mo in cyan. The FDH cofactors are distinguished by their reported oxidation states (IV: triangles, VI: diamonds). Reproduced with permission from ref. 88. Copyright 2022 American Chemical Society.

Despite comparable functions between EBDH and Fe(II)/α-ketoglutarate-dependent oxygenases, QM and QM/MM calculations combined with experimental kinetic isotope effect (KIE) studies found that EBDH likely acts via a carbocation intermediate, in contrast to the radical intermediates observed in Fe(II)/α-ketoglutarate-dependent oxygenases.[91-93] The proposed mechanism for EBDH starts with the homolytic cleavage of the target C–H bond with simultaneous transfer of a proton from a hydrogen-bonded histidine (His192) to the oxo ligand leading to a cationic substrate and a complex with an aqua ligand while the Mo(VI) center is reduced to Mo(IV). The second step includes rebound of a hydroxyl group to the substrate while His192 is re-protonated. Therefore, besides different reactive intermediates, another mechanistic difference between EBDH and Fe(II)/α-ketoglutarate-dependent oxygenases is that for EBDH, the reduction of the metal center happens via one step, while for Fe(II)/α-ketoglutarate-dependent oxygenases, the metal center is reduced in two steps.[94] However, there is evidence that not all Mo/W-containing enzymes have this feature. A closely related enzyme, steroid C25 dehydrogenase, which hydroxylates the C25 atom of a sterol aliphatic side-chain, appears to use different chemistry.[94] Unlike the proposed mechanism for EBDH, QM only, QM/MM, and KIE studies of the enzyme active site suggest a radical-rebound-like mechanism for steroid C25 dehydrogenase, analogous to the mechanism observed in Fe(II)/α-ketoglutarate-dependent oxygenases.[95]

### *2.5 Experimental Techniques Used for Enzyme Characterization*

High-valent Fe(IV)-oxo moieties are key intermediates formed during C–H activation by heme and non-heme iron enzymes, and their stability or orientation influences reaction

selectivity.[5] Nevertheless, this Fe(IV)-oxo moiety is notoriously challenging to isolate, owing to its fleeting lifetime on the order of a few seconds.[96] It has not been possible to structurally characterize the highly reactive Fe(IV)-oxo intermediates of enzymes by X-ray crystallography. Furthermore, dependence of non-heme enzymes such as SyrB2 on carrier proteins has impeded structural characterization of enzyme–substrate complexes.[97] Challenges with crystallographic characterization have led to a host of spectroscopic studies to understand metalloenzyme active-sites.[56, 98-100] While a variety of spectroscopic tools are used for experimental characterization, these methods rely heavily on DFT for interpretation.

Hyperfine sublevel correlation (HYSCORE) spectroscopy in combination with continuous-wave electron paramagnetic resonance (CW-EPR) spectroscopy has been used to characterize ligand coordination at the Fe(II)/α-ketoglutarate active-site of TauD.[98] McCracken *et al.* found two Fe(II) species that differ in NO coordination, where NO is frequently used as a spectroscopically sensitive surrogate for reactive $O_2$, and the placement of α-ketoglutarate ligands.[98] By measuring hyperfine couplings between the substrate and the Fe(II)-NO SyrB2 active-site, Martinie *et al.* found that a long Fe–methyl distance between Fe and the threonine substrate with a nearly perpendicular His–Fe–methyl angle selectively promotes native substrate chlorination overhydroxylation.[56] Mehmood *et al.* carried out experimentally guided molecular dynamics simulations using HYSCORE restraints to understand how substrate positions influence selectivity in non-heme halogenases.[47, 61]

Nuclear resonance vibrational spectroscopy (NRVS), interpreted using DFT, is also used for structural assignment[8-10] and understanding ligand environment effects on both heme[101] and non-heme[5, 99] Fe enzyme active-sites. NRVS and DFT have also been used to compare HAT reaction barriers between TauD and SyrB2 Fe(IV)-oxo intermediates[102] and explain how a

weaker Fe-oxo bond relates to higher reactivity of intermediates using model complexes.[99] Bioinspired transition-metal–oxo complexes are frequently synthesized and structurally characterized by EPR, Raman, UV/Vis, and nuclear magnetic resonance (NMR) spectroscopies to understand metalloenzyme reactivity.[11, 100] In particular, Mössbauer spectroscopy combined with DFT-computed spectral values can uniquely assign oxidation and spin states of Fe(IV)-oxo compounds[11, 100] and has been directly used for characterization of several α-ketoglutarate-dependent non-heme Fe enzymes.[103]

*3. Transition-Metal Complexes*

Single-site catalysts such as TMCs represent promising synthetic analogues to metalloenzymes, replicating the atom economy and selectivity of the metalloenzymes while providing a tunable ligand environment. Mononuclear TMCs with Fe centers have been a focus of design efforts due to the presence of Fe in metalloenzyme active sites (see Sec. 2). As ligand design has evolved from bioinspired porphyrin ligands to non-heme nitrogen coordinating ligands to carbene or oxygen coordinating ligands, computational studies have proven indispensable in understanding metal–ligand bonding and C–H bond activation energetics. Furthermore, QM studies have uncovered the role of oxidation and spin-state dependence for C–H bond reactivity that is impossible to investigate experimentally.

*3.1 The Development of the "Oxo Wall" Theory*

Metal-oxo intermediates of metalloenzymes that perform C–H activation inspired the synthesis of TMCs with metal-oxo moieties. Gray and coworkers proposed the “oxo wall” for tetragonal metal-oxo compounds to explain why earlier (e.g. V, Cr) transition-metal–oxos form more readily than later (e.g. Mn, Fe, Co) transition-metal–oxos.[104-105] They proposed that only metals with five or fewer *d*-electrons could form terminal metal-oxo intermediates with multiple-

bond character.[104, 106] Furthermore, the spin state of a 3*d* transition-metal–oxo complex affects its metal-oxo formal bond order and thus its stability.[104, 107] Many compounds near this "oxo wall" (e.g. high-valent Fe and Co) are highly reactive and only observed in the gas phase, requiring DFT for interpretation of their reactivity.[108-109]

*3.2 P450-Inspired Transition-Metal Complexes*

The identification of Fe-oxo active sites in enzymes led to intense synthesis efforts for TMCs that could form Fe-oxos.[110-111] Initial studies on P450-inspired Fe-oxo compounds focused on porphyrin ligands to understand the role of spin and TSR for C–H bond reactivity[112] (Figure 8). Porphyrins, comprised of four pyrroles joined by methylene bridges, stabilize high-valent metal-oxo intermediates. These ligands motivated the design of corroles and corrolazines, which are also comprised of pyrroles but joined by three methylene or aza bridges respectively (Figure 8).[113-114]The distinct electronic structure of these ligands alters C–H bond reactivity and underscores the role of ligand design in controlling reactivity.[113-114] Here, DFT has been essential for understanding both the relationship between substrate bond strengths and C–H activation barrier heights[114] and between ligand structure and TMC spectroscopic properties.[113]

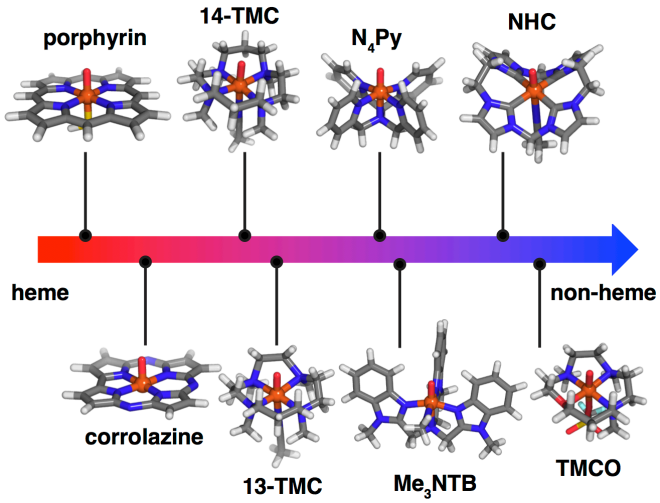


**Figure 8.** Eight representative transition-metal complex catalysts that have been studied for C–H bond activation reactivity. All structures are shown as Fe(IV)-oxo intermediates, and range from

heme-like (left) to non-heme-like (right): Fe(IV)=O(porphyrin)(SH), Fe(IV)=O(corrolazine), Fe(IV)=O(14-TMC)($CH_3CN$) (14-TMC = 1,4,8,11-tetramethyl-1,4,8,11-tetraazacyclotetradecane), Fe(IV)=O(13-TMC)($CH_3CN$) (13-TMC = 1,4,7,10-tetramethyl-1,4,7,10-tetraazacyclotridecane), Fe(IV)=O($N_4Py$) ($N_4Py$ = *N,N*-bis(2-pyridylmethyl)-*N*-bis(2-pyridyl)-methylamine), Fe(IV)=O($Me_3NTB$)($CH_3CN$) ($Me_3NTB$ = tris-((*N*-methyl-benzimidazol-2-yl)methyl)amine), Fe(IV)=O(NHC)($CH_3CN$) (NHC = 3,9,14,20-tetraaza-1,6,12,17-tetraazoniapenta-cyclohexacosane-1(23),4,6(26),10,12(25),15,17(24),21-octaene), and Fe(IV)=O(TMCO)(OTf) (TMCO = 4,8,12-trimethyl-1-oxa-4,8,12-triazacyclotetradecane, OTf = triflate) Structures are shown with Fe in brown, C in gray, N in blue, O in red, F in cyan, S in yellow, and H in white.

### *3.3 Transition-Metal Complexes Inspired by Non-Heme Iron Enzymes*

Numerous synthetic studies have extended beyond hemes. The high frequency of Fe coordination by N in enzymes inspired other N-coordinating ligand scaffold designs. Rohde *et al*. successfully stabilized an Fe(IV)-oxo for the first crystallographic characterization of a non-heme terminal metal-oxo complex, which used a cyclam ligand[14] (Figure 8). This example demonstrated that neutral nitrogen atoms, as opposed to anionic porphyrinic nitrogen atoms, could also stabilize a metal-oxo moiety. Correspondingly, Cho *et al*. explored the effects of cyclam ring contraction on Fe(IV)-oxo reactivity and used DFT to correlate geometric structure to C–H activation barrier heights[115] (Figure 8). DFT calculations enhanced understanding of how reaction and spin state energetics vary as a function of ligand field strength.[107, 116-117] Identification of a HS Fe-oxo intermediate in the non-heme Fe(II) enzyme TauD[9] by Mössbauer spectroscopy motivated intense efforts to isolate a synthetic HS Fe-oxo compound.[13] Despite the isolation of landmark Fe(IV)-oxo compounds such as ($N_4Py$)Fe(IV)-oxo, HS metal-oxo TMCs remained elusive, limiting experimental validation of the role of spin in reactivity[12] (Figure 8).

### *3.4 Understanding the Role of Spin and TSR*

The principles of TSR[118] and exchange-enhanced reactivity[119] (EER), derived from DFT studies, were essential in explaining the lower C–H activation barrier heights of a HS metal-oxo

and the selectivity ratios between hydroxylation and epoxidation products. DFT calculations revealed that a weaker ligand field would facilitate access to a HS metal-oxo and motivated the design of bulkier ligand scaffolds that weaken the ligand field strength.[117, 120] Although bulkier ligands did indeed form HS metal-oxo compounds, they exhibit sluggish reactivity typically attributed to steric effects that prevent substrates from reaching the active site.[120] TSR is used to explain increased C–H bond reactivity in cases where bulky ligands weaken the ligand field but do not change the ground spin state. Seo *et al*. designed $Me_3$NTB, a ligand that has P450-like reactivity despite stabilizing an intermediate-spin (IS) triplet metal-oxo[121] (Figure 8). Because TSR challenges the interpretation of IS Fe(IV)-oxo reactivity, a joint DFT/CASSCF and experimental study found that using N-heterocyclic carbene (NHC) ligands promotes triplet-only reactivity that was found to be comparable to complexes exhibiting TSR[122] (Figure 8). This study called into question whether TSR alone can always explain improved C–H bond reactivity.

*3.5 Probing Other Bioinspired Active Sites*

Although N-coordinated Fe(IV)-oxo moieties have been the primary focus of study, Monte Peréz *et al*. introduced oxygen coordination into a cyclam, inspired by the oxygen-rich coordination environments observed in non-heme enzymes.[123] Consequently, they experimentally measured a 10-fold increase in C–H bond reactivity (Figure 8). Beyond ligand design, Wang *et al.* isolated a Co terminal oxo compound and studied its electronic structure using DFT and CASSCF calculations to assign a quartet ground state. While Co-oxos would be expected to have increased C–H bond reactivity according to the oxo wall theory, reduced reactivity was instead observed compared to Fe(IV)-oxos.[124] This observation could be attributed to the fact that this structure was not in a tetragonal geometry and thus the oxo wall theory was not applicable.[124] In contrast, Mn(IV)-oxo compounds, which should have more stable metal-oxo

moieties according to the "oxo wall" theory, show comparable C–H bond reactivity to Fe(IV)-oxo compounds despite differences in spin states and electron configurations.[125-128] DFT and CASSCF studies found that HAT barriers are comparable between Mn and Fe compounds, emphasizing that Mn compounds are underexplored for C–H bond reactivity.[127] Nandy *et al.* recently explored a space of 16 million TMCs for C–H activation without assuming an N- or O-containing primary coordination sphere and found that low-spin Fe(IV)-oxo compounds with strong-field (e.g. P- or S-coordinating) ligands have the best tradeoff between HAT energetics and methanol release[129] (Figure 9). Yadav *et al.* have recently designed Fe TMCs to obtain product halogenation selectivity only seen in enzymes.[22] Here, calculations found that active site steric bulk affects C–H activation kinetics and halogenation selectivity.[21]

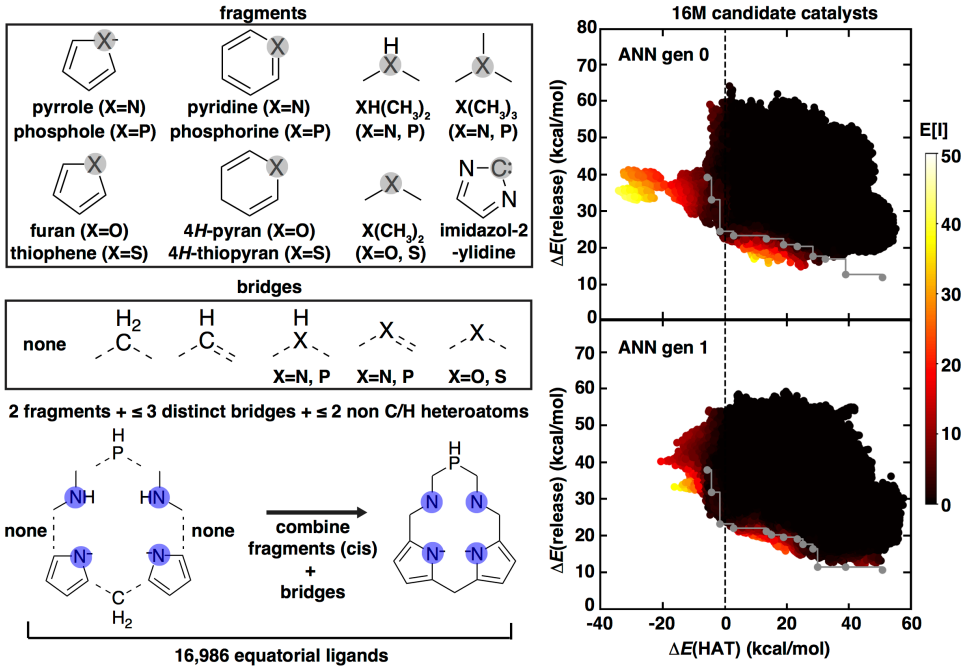


**Figure 9.** (left) Fragments and bridges that comprise tetradentate macrocycles for catalysis when combined with Mn and Fe. (right) two-dimensional expected improvement (2D-EI) scores from artificial neural network (ANN)-driven exploration over two generations of a multimillion-catalyst space while screening for ΔE(HAT) and ΔE(release). A Pareto front as computed by DFT for catalysts with the optimal tradeoff between the two reaction energies is noted in gray. Reproduced with permission from ref. 129.

*3.6 C–H Bond Activation Pathways, Oxidation State Dependence, and Selectivity*

The critical intermediates in C–H bond activation are challenging to isolate experimentally.[20, 130-131] Consequently, DFT calculations have been essential for quantifying the role of spin in mechanism[20, 130-131] and reactivity.[107] These computational studies have found that reactivity trends are dominated by spin state. Geng *et al*. used DFT calculations to quantify oxidation-state dependence and found that differences in oxidation state explained differences in C–H bond activation propensity for compounds with comparable ligand fields.[132] Oxidation states or TSR, however, cannot explain post-C–H activation selectivity for rebound or dissociation. Reactive mode composition factor (RMCF) analysis is an energy decomposition method that can be used to explain product selectivity by analyzing the kinetic energy distribution in a TS. Maldonaldo-Dominguez and Srnec used DFT and RMCF analysis to quantify when a substrate will rebound or dissociate.[133] This understanding can improve the high-throughput virtual screening (HTVS) of catalysts with higher selectivity.

*3.7 C–H Bond Activation Mechanisms and Bond Dissociation Free Energies (BDFEs)*

Metal-oxo moieties observed in enzymes and transition-metal complexes activate strong C–H bonds (i.e., with high dissociation energies) such as methane (105 kcal/mol) via a HAT step.[134-135] As described previously, the HAT step is a concomitant transfer of one proton and one electron from a substrate to the oxidant, a metal-oxo moiety.[136-137] Metal-oxo complexes have HAT kinetic barriers that tend to correlate with the substrate C–H bond dissociation free energy ($BDFE_{C–H}$)and the $BDFE_{O–H}$ of the post-reduction oxidant species.[138] The relationships between $BDFE_{C–H}$, $BDFE_{O–H}$, reduction potential, and basicity of the metal-oxo moiety are typically represented using a thermodynamic cycle[139] (Figure 10). This thermodynamic square represents

three potential mechanistic pathways: stepwise proton-coupled electron transfer (PCET), mechanisms initiated either with electron transfer (ET/PT) or proton transfer (PT/ET), and concerted proton electron transfer (CPET).[140] For PT/ET and ET/PT, the rate-determining step involves PT and ET respectively, whereas both PT and ET are involved in the rate-determining step for CPET. Within this framework, the CPET mechanism is categorized as either synchronous, with equal contribution of PT and ET in the TS, or asynchronous, with the domination of either PT or ET.[141]

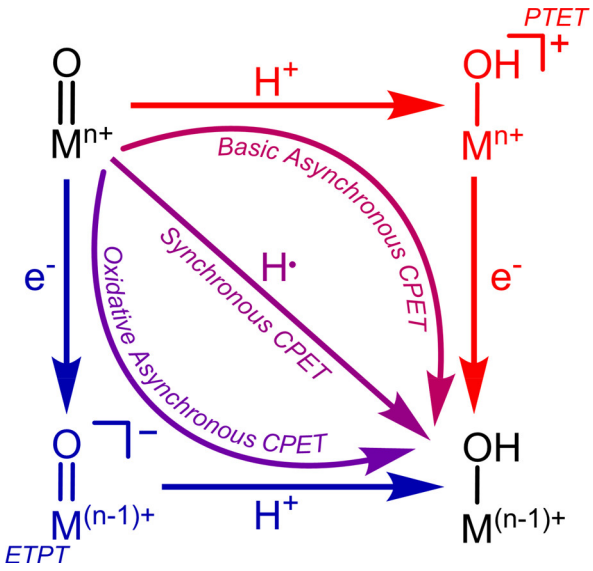


**Figure 10.** A thermodynamic square for the proton-coupled electron transfer (PCET) mechanism including stepwise (PTET or ETPT) and concerted (CPET) proton and electron transfer. Reproduced with permission from ref. 142. Copyright 2019 American Chemical Society.

Several experimental and computational studies on heme[114, 143] and non-heme metal–oxo-like Fe(IV)-oxo[116, 144-145], Ru(IV)-oxo[146], Mn(IV)-oxo[128], Cr(V)-oxo[147] complexes with various substrates indicate a linear correlation between BDFE and the log transformation of the HAT reaction rate constant ($k_{C–H}$). These systems that show strong linear correlations between $\log(k_{C–H})$ and $BDFE_{C–H}$ follow a Bell–Evans–Polanyi (BEP)-like correlation because $\log(k_{C–H})$ represents the HAT barrier by an Arrhenius relation.[148-149] Several studies report concerted but

asynchronous transfer of the electron and proton for various metal-oxo systems including Fe(V)-oxo[150], Mo(V)-oxo[151], Co(III)-oxo[142], Ru(IV)-oxo[152], Cu(III)-$O_2CAr$[153], and Mn(IV)-oxo[154] complexes. The dominant role of PT in C–H homolytic bond cleavage was found to be important in all of these studies, thus underscoring the importance of the basicity of the metal-oxo species. In addition to studies on the relationship between thermodynamic parameters and asynchronicity of C–H bond activation, there has also been effort to quantify the role of other metal-oxo properties, such as spin density and spin state.[107, 155-158] These studies show spin- density and spin-state dependence of oxo formation, HAT, and reactivity. Recently, a consensus statistical analysis of C–H activation by a large number of metal-oxo complexes was carried out by considering all thermodynamic properties as well as structural and electronic properties computed by DFT.[159] By considering all properties statistically, this study revealed that only thermodynamic ($\Delta G_{PT}$, $\Delta G_{ET}$, $\Delta G_{CPET}$) parameters play important roles in the C–H bond reactivity of metal-oxo complexes, indicating that HAT is thermodynamically controlled. Although this conclusion was reached on a set of metal-oxo complexes, some catalysts show strong kinetic isotope effects (KIEs) during C–H activation, implying that hydrogen atom tunneling must be considered in some cases.[160-162]

*4. Heterogeneous Catalysts*

Heterogeneous catalysts have been instrumental in the industrial valorization of chemical feedstocks due to their robustness, low operating costs, and easy separation from reactants and products. Catalysts such as zeolites, MOFs, and SACs offer similar active site tunability to TMCs but the scalability of bulk-metal catalysts. Here, Fe-doped zeolites, MOFs, and SACs have been used for light alkane oxidation. Due to challenges in experimental materials characterization, DFT has played a key role in corroborating spectroscopic studies and

uncovering the role of chemical environment on C–H bond activation with atomic precision. These studies have led to comparisons between heterogeneous catalyst active sites and TMCs or metalloenzyme active sites.

*4.1 Zeolites*

Zeolites are a class of microporous materials with repeating $TO_4$ tetrahedra (where T is typically Si or Al) that form the secondary building units (SBUs) which further combine into distinct framework topologies.[163] The inner-pore structure of zeolites can accommodate extra-framework transition-metal ions that constitute well-defined catalytic active sites, drawing direct analogies to metalloenzymes[10, 164-165] (Figure 11). Unlike most enzymes, zeolites are highly stable, even under extreme conditions, which make them viable catalysts for industrial applications.

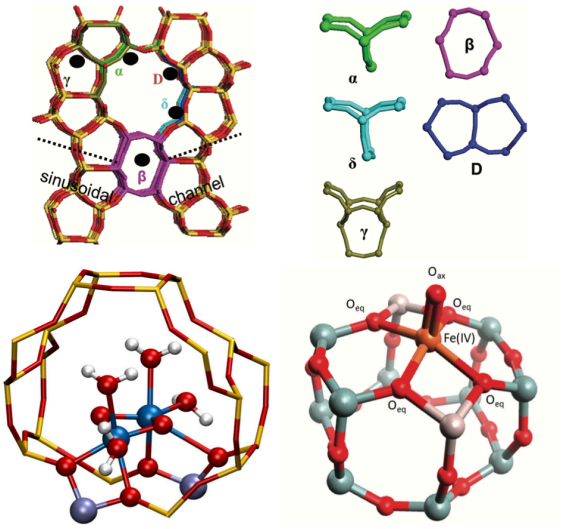


**Figure 11.** (top) Structure of a representative zeolite topology (ZSM-5) showing possible cation sites where extra-framework metal ions can be incorporated. Si atoms are shown in yellow and O atoms are shown in red. Green, purple, light blue, dark blue, and yellow-green highlights represent extra-framework cationic sites. (bottom left) Cluster model of a di-iron active site contained within the ZSM-5 zeolite pore. Si atoms are shown in yellow, Al in purple, Fe in blue, O in red, and H in white. (bottom right) Cluster model of a mononuclear Fe-oxo intermediate in the CHA zeolite. Si atoms are shown in gray, Al in peach, Fe in brown, and O in red. Structures adapted with permission from refs. 164-166. Copyright 2018, 2012 and 2018 American Chemical Society respectively.

In the early 1990s, Pannov *et al*. first showed that zeolites with isolated Fe sites undergo C–H bond activation reactivity.[167] Here, analysis of the outcomes of stoichiometric reactions with an $N_2O$ terminal oxidant indicated the role of a highly active Fe-oxo species in the activation of light alkanes (Scheme 1). The nature of the reactive Fe-oxo species, however, remains under debate. Magnetic circular dichroism (MCD) and NRVS complemented by DFT modeling of Fe-zeolites revealed a HS mononuclear square planar Fe(II) site contained in the zeolite pore which forms a HS Fe(IV)-oxo species upon interaction with $N_2O$[168-169] (Figure 11). The Fe-oxo bond is extremely strong and yet still highly reactive due to its constrained coordination geometry surrounded by weak-field ligands. Other studies performing EXAFS supported by DFT simulations reveal a di-iron site with two antiferromagnetically coupled HS Fe(III) centers, where oxidation using $H_2O_2$ forms a terminal Fe-oxo species on one of the Fe sites[170] (Figure 11). On the other hand, analogous Cu-zeolites have shown similar activity towards C–H activation where the reactive Cu-oxo can be formed with $O_2$.[171-172] Activity with $O_2$ as the oxidant has only recently been observed in Fe-zeolites, where two adjacent isolated Fe atoms are believed to participate in $O_2$ splitting to form two terminal Fe-oxo sites.[173-174] Nonetheless, spectroscopic measurements interpreted by DFT studies have argued for both dinuclear and trinuclear Cu-oxo clusters as the C–H activation active site.[175-177]

**Scheme 1.** Radical rebound catalytic cycle for partial oxidation of methane to methanol. The metal (M) of the resting state catalyst (1) starts in oxidation state II/III. $N_2O$ is used as a terminal oxidant to form a high-valent metal-oxo intermediate (2) in oxidation states IV/V. This species then undergoes HAT to form the metal-hydroxo intermediate (3), which rebounds with the methyl radical to form the methanol-bound intermediate (4), which is then released from the catalyst.Reproduced with permission from ref 178. Copyright 2022 Springer Nature.

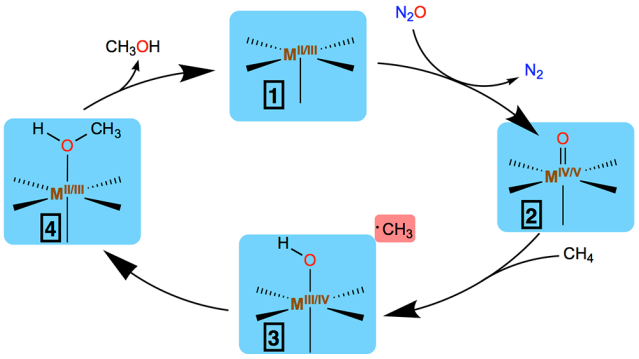


*4.2 Metal-Organic Frameworks (MOFs)*

MOFs are another class of microporous reticular materials comprising an inorganic node (i.e., an SBU) coordinated to organic linkers[179] (Figure 12). The metal ions in the SBU are site-isolated, and many common organic linkers are weak-field ligands (e.g., N- or O-coordinating).[180] For SBUs containing coordinatively unsaturated mid-row 3*d* metals that can serve as active sites for catalysis, the weak-field ligands induce HS configurations, also making the active sites amenable for redox reactivity.[181-182] Like zeolites, many of the structural and electronic features of the MOF active sites have been described as analogous to metalloenzymes,[180] motivating them as good candidates for bioinspired C–H activation. Concerted effort in MOF synthesis and characterization has resulted in over 70,000 synthesized MOFs with a high degree of elemental and compositional diversity.[183-184] Additionally, these MOFs are highly tunable, unlike zeolites, allowing for post-synthetic modification to functionalize the SBU or linker and enhance catalytic activity.[185]

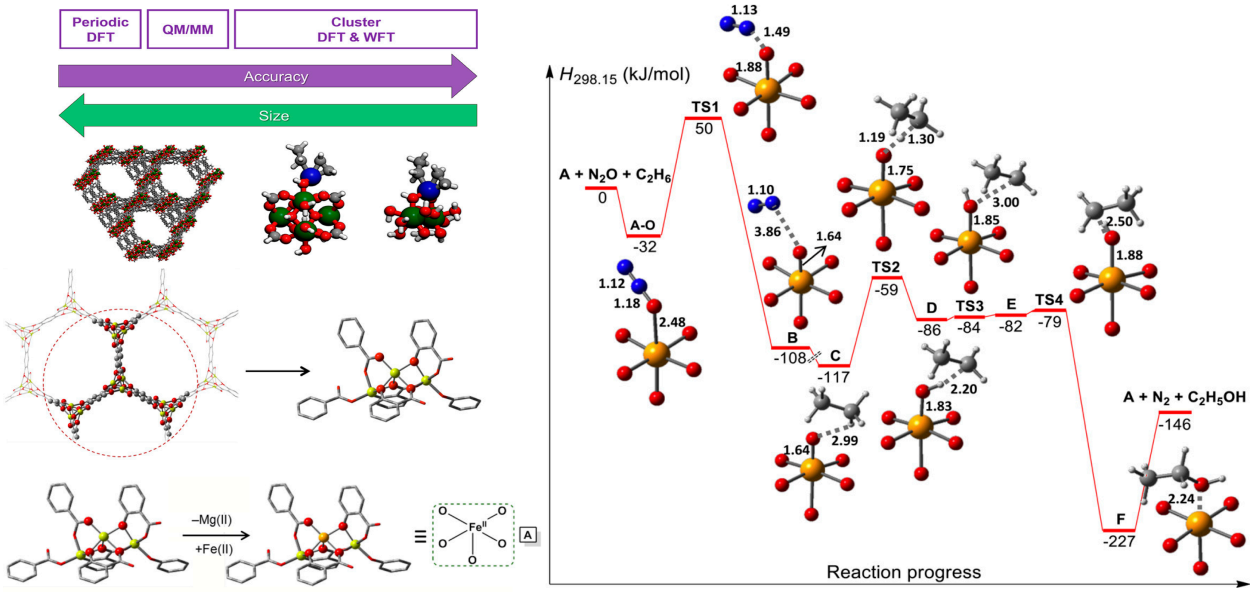


**Figure 12.** (top left) Computational modeling of MOFs: a size–accuracy tradeoff ranging from the largest and least accurate models for periodic DFT to small but accurate models for cluster DFT and WFT. Zr atoms are shown in green, in red, C in gray, H white, and generic metal atoms are shown in blue. (bottom left) Extended structure of Mg-MOF-74 showing the extracted 88-atom cluster model used for DFT. The central square pyramidal Mg site in the cluster model was replaced with Fe to serve as the active site for ethane hydroxylation. Mg atoms are shown in light green, Fe in brown, O in red, and C in gray. (right) DFT-derived enthalpy profile, $\Delta H_{298.15}$ (kJ/mol), for ethane hydroxylation using $N_2O$ as an oxidant at the Fe active site in the Mg-diluted Fe-MOF-74 cluster model. Inset structures show changes at the Fe active site during the reaction where the rest of the cluster has been omitted for clarity. Fe atoms are shown in brown, O in red, N in blue, C in gray, and H in white. Accuracy and size schematic adapted with permission from ref. 186. Copyright 2018 American Chemical Society. Cluster model schematic and energy landscape diagram adapted with permission from ref. 187. Copyright 2015 American Chemical Society.

The vast size of MOF chemical space limits performing experimental catalytic studies making computational modeling essential to guide rational design of MOFs for catalysis.[186] The cost–accuracy tradeoff governs the approach chosen to model MOFs, which are porous and have large fractions of void space. Periodic DFT, typically with a generalized gradient approximation (GGA) functional, is often used to model the structural properties of these materials.[186, 188] GGA functionals like PBE predict optimized structures reasonably well but may not accurately predict band gaps or spin state ordering in 3*d* transition-metal MOFs. Thus, to overcome the cost–accuracy tradeoff presented by periodic DFT, many studies model local properties at the active

site via global hybrid DFT or multiconfigurational wavefunction theory on cluster models in which the SBU is extracted and capped to mitigate the computational cost of using more accurate methods.[186] Because cluster models may lead to truncation effects, QM/MM has also been used to model the MOF active site within its native scaffold, rendering a more realistic description of MOF architecture. This approach preserves accuracy through usage of larger basis sets and hybrid functionals to model the reactive portion using QM and MM to model the rest of the MOF[189-190] (Figure 12).

DFT studies with cluster models have provided mechanistic insights into light alkane hydroxylation on Fe-MOFs with an $N_2O$ oxidant.[181, 191] Fe-MOF-74 hydroxylates ethane via a radical rebound mechanism at an HS Fe(II) center. The Fe active site is ligated by weak-field ligands in a constrained coordination environment enforced by the extended MOF structure, resulting in the formation of a stable terminal Fe(IV)-oxo with high reactivity for C–H activation.[181] Here, $N_2O$ activation to form the terminal Fe(IV)-oxo was found to be rate-limiting[187] (Figure 12). Propane hydroxylation over MIL-100(Fe) also found $N_2O$ activation to be rate-limiting in a radical rebound mechanism, which was further confirmed by a kinetic study.[191] A recent study, however, performed in-situ FTIR measurements of methane oxidation over PCN-250 found vibrational peaks, corroborated by DFT, that are characteristic of a stable methoxy species at the Fe active site, which cannot be explained by the rebound mechanism.[192] This highlights the lack of clarity on the precise mechanism, echoing some of the debate regarding C–H activation observed in metalloenzymes and zeolites.[166]

MOFs have considerable potential for catalysis owing to the presence of open metal sites on many MOF SBUs. Furthermore, MOFs have additional useful structural features that could also be exploited to augment catalytic activity.[193] For instance, shape selectivity in MOFs has

been observed to enhance selectivity for methane functionalization without overoxidation[194], whereas molecular analogues led to overoxidized products.[195] MOFs are prone to defect sites arising from missing or modified linkers and nodes.[196-197] Several studies indicate a substantial positive correlation of catalytic activity with the number of engineered defect sites in MOFs.[198-199] In general, computational and data-driven studies can play a key role in exploring large MOF databases and identifying structure–property relationships in MOFs for catalytic activity. Nevertheless, several key properties of ideal MOF catalysts, such as stability, can be challenging to predict with purely computational modeling. Efforts of screening MOFs for catalysis have already been made with ML workflows developed by Nandy *et al*. to predict MOF stability for catalytic applications, a property which can be very challenging to predict from first principles.[200]

*4.3 Single-Atom Catalysts (SACs)*

SACs are emergent catalysts that are effective for catalyzing small-molecule activation reactions. SACs show promise for combining the active site tunability of homogenous catalysts and the scalability of the heterogeneous catalysts. The N-doped graphene SACs[201-202], where an isolated metal atom is embedded in a graphitic carbon material, are most transparently analogous to their homogeneous counterparts in comparison to other (e.g., single metal atoms on metal oxides) classes of SACs. The Fe-$N_4$ active site in Fe-SACs was proposed in analogy to hemes[203-205], where the Fe atom is also coordinated to four nitrogen atoms.

Various experimental characterization techniques have been used to investigate SAC structures and reactivity, especially in the case of iron. For example, the properties of Fe are characterized by $^{57}$Fe Mössbauer spectroscopy[206-207], X-ray absorption near-edge spectroscopy (XANES), and EXAFS.[208-209] High-angle annular dark-field scanning transmission electron

microscopy (HAADF-STEM)[210-211] is frequently utilized to confirm that metals are atomically dispersed in SACs. These spectroscopic analyses suggest that the support and primary coordination sphere are essential in determining catalytic reactivity[212-213], consistent with conclusions drawn from DFT simulations.[214-215] Joint experimental characterization and computational studies have highlighted the roles of the support and primary coordination sphere for SACs in catalyzing HER[216], ORR[217-219], $CO_2$RR[209, 220-221], and selective C–H bond oxidation.[207, 222]

It remains a challenge, however, to uncover the origin of the SAC reactivity by experiment alone. Both spectroscopic techniques[210, 223] and DFT calculations[211, 224] have suggested that the Fe–support interaction can change under operating conditions. Besides structural changes during the reaction, the electronic properties of the active site remain elusive[210, 224] (Figure 13). Similar to biological catalysts or TMCs, the spin and oxidation states influence SAC reactivity.[225] Gu *et al.* found that Fe(III) does not get oxidized or reduced during the electrocatalytic reduction of $CO_2$ to CO, which contributed to the greater activity of Fe(III) relative to conventional Fe(II) sites.[226] The $^{57}$Fe Mössbauer spectroscopic studies necessary to assign the precise oxidation/spin states of the $FeN_xC_y$ moiety remain challenging due to the distribution of sites that must be obtained from spectral fits.[206, 227] Typically, SACs are modeled with plane-wave, semi-local DFT, in which the metal oxidation and spin states are either erroneously predicted or not precisely defined(i.e., due to fractional occupation of frontier states with smearing using semi-local DFT). To reveal the electronic structure of the metal and its relationship to the catalytic reactivity, efforts to understand SAC reactivity via molecular mimics have probed the effects of nitrogen type (e.g. pyridinic or pyrrolic), typically embedded in 14- or

16-membered macrocycles.[208, 228-229] DFT modeling of finite size nanoflakes that represent the infinite system also help address the challenges in periodic systems.[24]

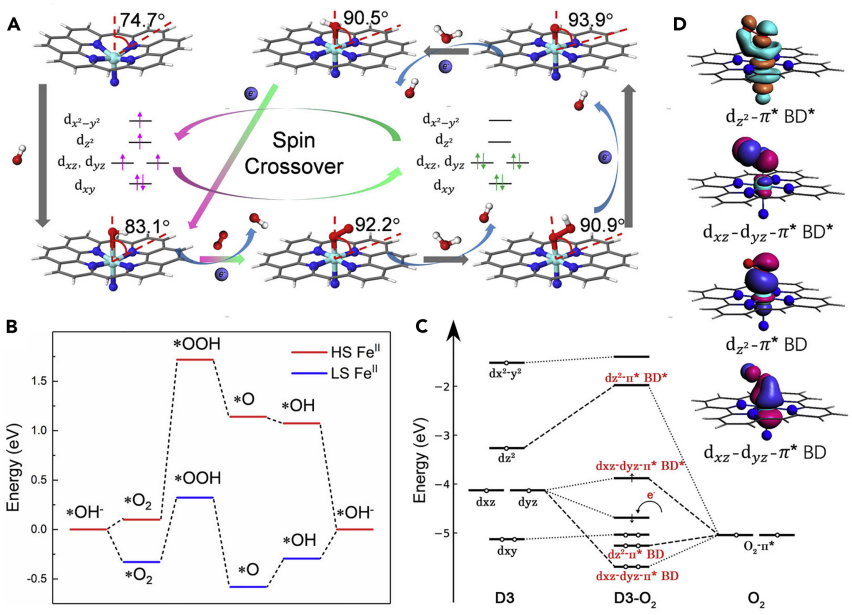


**Figure 13.** (A) Structures and electron configurations for the N–$FeN_4C_{10}$ moiety in ORR, (B) potential energy profiles with (blue) and without (red) spin crossover during ORR in alkaline media, (C) molecular orbital diagram between N–$FeN_4C_{10}$ and $O_2$, and (D) molecular orbital isosurfaces for frontier orbitals. Reproduced with permission from ref. 224. Copyright 2020 Elsevier.

DFT has also been a useful tool for mechanistic understanding[230-231] and fast screening of new SACs.[232-233] Density functional approximation (DFA) sensitivity[234] and improved electronic structure methods for accurate descriptions of spin- and oxidation-state-dependent properties[235], however, remain active areas of research (see Sec. 5). Additionally, HTVS and ML are promising approaches that can be leveraged to elucidate structure–reactivity relationships in SACs and to study the potential role of structural changes during reactions.

*5. Unifying Themes Across All Catalysts*

The metal-oxo moieties that activate C–H bonds in metalloenzymes have inspired the design of TMCs and heterogeneous catalysts as targets for high-throughput screening. DFT-

driven screening enables *in silico* design of bioinspired catalysts. Scaling relations that draw relationships between catalyst thermodynamics and kinetics reduce the number of calculations necessary to evaluate a catalyst, which facilitates low-cost screening of large chemical spaces. These widely employed scaling relations seldom hold over large datasets of TMCs, mandating more general tools for HTVS. At the same time, scaling relations may be sensitive to functional choice, leading to method-dependent conclusions. Catalysts with complex electronic structure will require methods beyond DFT for their accurate evaluation. NCIs that influence catalyst selectivity can also be understood by computational studies and engineered for improved catalyst design, but NCIs are notoriously challenging to address with most conventional modeling tools. ML-driven catalyst design has reduced reliance on linear relationships and on computed descriptor variables, unlocking the high-throughput screening of multimillion compound spaces.

*5.1 Scaling Relations and Strategies to Break Them*

Exhaustive screening of catalyst energy landscapes with DFT is challenged by the fact that computational cost scales linearly with both the size of the design space and the number of reactive intermediates. To address this, one can use Bronsted–Evans–Polanyi (BEP) relationships between activation energies and reaction energies and linear free energy relationships (LFERs) between distinct thermodynamic steps to draw linear relationships between a DFT-computed "descriptor" variable and reaction kinetics or thermodynamics. These relationships can be combined to construct "volcano plots" that relate the descriptor to the best achievable catalyst thermodynamics or kinetics, thereby accelerating catalyst discovery. Catalysts at the top of the volcano plot have high activity and do not bind any single intermediates too weakly or tightly. Although these relationships reduce the number of necessary calculations by using a descriptor variable that is linearly correlated to reaction energies or barrier heights, the most appropriate

descriptor and its relationship to key properties are rarely known beforehand. While potential disruptions in scaling relations necessitate explicit calculation of intermediates, they provide opportunities for overcoming kinetic or thermodynamic limitations in catalyst design.

DFT-derived universal BEP relationships for C–H activation have been developed to describe how the C–H activation barrier height correlates linearly with the HAT reaction energy over a diverse space of both homogeneous and heterogeneous catalysts, independent of catalyst geometry.[236-237] Furthermore, the barrier heights for the activating the first and second C–H bond on the same molecule have a 1:1 relationship for a wide range of catalysts, implying a selectivity–conversion limit for hydroxylated products on heterogenous catalysts.[238] The HAT BEP relationships have been extended to homogeneous catalysts, where thermodynamic descriptors such as HAT reaction energies and PCET free energies can predict HAT barriers for transition metal-oxo complexes[129, 157, 159], independent of other structural or electronic parameters such as spin state, steric environment, or oxygen radical character.[159, 239] (Figure 14). These BEP relationships eliminate the need to perform computationally demanding TS calculations to obtain HAT barriers. This in turn enables faster computational catalyst screening.

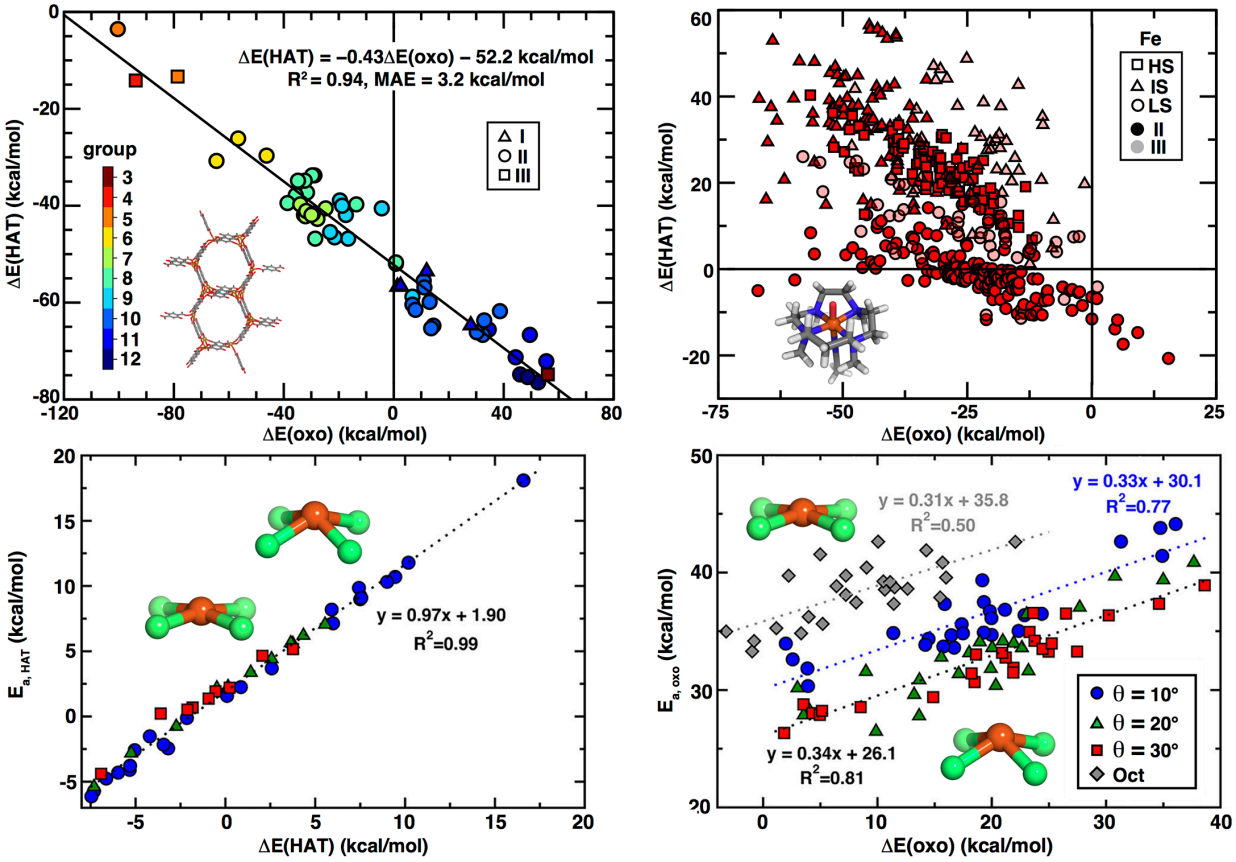


**Figure 14.** (top left) LFER between oxo formation and HAT over 60 MOF catalysts. Compounds are colored by group number for metal in the MOF and have shapes corresponding to formal oxidation state. Inset structure is Fe-MOF-74, with Fe in brown, O in red, C in gray, and H in white. $H_2$ is used as the reference substrate for HAT. Triplet $O_2$ is used as the reference for oxo formation. (top right) LFER for oxo formation and HAT across Fe transition metal complexes with diverse ligand chemistry. The compounds are distinguished by their spin states: LS (circle), IS (triangle), or HS (square) and oxidation state (translucent for M(III) and solid for M(II)). $CH_4$ is used as the reference substrate for HAT. $N_2O$ is used as the reference for oxo formation. (bottom left) BEP relationship for HAT for a set of distorted square planar minimal model catalysts with varying metal out-of-plane distortion. (bottom right) BEP relationship for oxo formation on distorted square planar minimal model catalysts. MOF LFER figure adapted with permission from ref. 23. Copyright 2019 American Chemical Society. Molecular LFER figure adapted with permission from ref. 107. Copyright 2020 American Chemical Society. BEP relations adapted with permission from ref. 157. Copyright 2018 American Chemical Society.

Although BEP relationships reduce the number of necessary explicit TS calculations, one may still need to calculate properties of many reactive intermediates to evaluate catalyst thermodynamics. LFERs constitute a framework for predicting thermodynamic quantities

associated with a catalytic cycle from a single descriptor thus alleviating computational costs. DFT studies have shown linear correlations between frontier orbital energies of mononuclear Fe-oxo intermediates and reaction energetics associated with light alkane hydroxylation, such as oxygen binding enthalpy, HAT enthalpy, and alcohol release enthalpy.[240] This idea was further applied in MOFs where inverse correlations exist between the oxo formation and HAT energies at the MOF node[23] while the 3*d* transition metal group number of the MOF node governs oxygen binding strength[241-242] (Figure 14).

Well-known scaling relations, however, are easily disrupted by changes to the catalyst structure[107, 157, 243-245] or may fail to hold across multiple metals in differing oxidation or spin states.[158] Here, DFT has played a crucial role in quantifying the effects of tensile and compressive strain on both heterogeneous catalysts[243] and TMCs.[107, 157, 246] In transition metal chemistry, strain or compression of metal–ligand bonds leads to variation along a BEP relationship or LFER. In contrast, BEP relationships and LFERs are both readily disrupted by out-of-plane geometric distortions of the metal with respect to ligands.[157] Gani *et al*. found that out-of-plane distortion improves metal-oxo formation kinetics for fixed oxo formation thermodynamics[157] (Figure 14). This distortion can also improve oxo formation thermodynamics without worsening HAT. In contrast, some BEP relationships (e.g., HAT BEP) are challenging to break, reinforcing the existence of a universal HAT BEP relation that is independent of geometry[129, 157, 236] (Figure 14).

Beyond the role of strain in catalysis, DFT is useful to isolate the role of spin in tuning or disrupting LFERs.[107, 158] Nandy *et al*. found that the linear correlations that were used by Liao *et al.* to screen Fe catalysts[240] were not general to multiple metals in different electron configurations.[158] Nandy *et al*. then demonstrated that LFERs show strong oxidation and spin

state dependence, due to differing effects of spin on different reactive intermediates[107, 158] (Figure 14). Correspondingly, a LFER that holds for HS Fe(II) does not generalize to low-spin (LS) Fe(II). Specifically the LFER for oxo formation vs. HAT will have a distinct slope and intercept depending on the spin state. While moderate scaling may hold within an individual spin and oxidation state, a single LFER does not hold strongly through all metal-oxidation-spin state combinations. Researchers can harness this lack of scaling to design catalysts that have a superior thermodynamic tradeoff.[158]

In addition to spin state and distortion that influence metal–adsorbate bonding, NCIs may disrupt LFERs via through-space interactions. DFT has been used to investigate the role of active-site-adjacent functional groups that have been installed in TMCs[157], zeolites[247], and MOFs[248], and has uncovered the role of NCIs in selectively stabilizing specific intermediates (e.g. the metal-oxo), thus disrupting LFERs. The advent of NCI-disrupted scaling has also led to the design of molecular hangman-like scaffolds[249-250] that promote through-space interactions that can overcome thermodynamic or kinetic limits.

*5.2 Sensitivity of Scaling Relations to Density Functional Approximation*

Semi-local DFAs such as GGAs underestimate reaction barriers due to self-interaction error.[251] Attempts to improve semi-local DFT predictions of barrier heights include incorporation of self-interaction-free Hartree–Fock (HF) exchange into hybrid DFAs.[251] Because hybrid DFAs are frequently used to study barrier heights and reactivity, it is useful to know the extent to which changing the HF exchange fraction in the functional changes property predictions. Toward that end, HF exchange sensitivity analysis has been employed to quantify the effect of the HF exchange fraction on barrier heights and reaction energies. Gani *et al*.[252] and Mahler *et al*.[253] found that increasing the HF exchange fraction in a global hybrid functional reduces barrier

heights in reactions where the hybridization decreases in the TS with respect to the reactants (Figure 15). Natural bond orbital (NBO) analyses on these reactions illustrated that HF exchange stabilizes bonds in the TS relative to bonds in reactants, leading to anomalous barrier lowering.[253] Additionally, symmetry breaking, singlet diradicals[254], and differences in delocalization as quantified by bond valence[252] have also been identified as contributing to cases where lower reaction barriers are predicted by hybrid functionals with respect to GGAs. One approach to achieve error cancellation has been proposed in which HF orbitals are used non-self-consistently in semi-local DFT calculations to improve barrier heights for HAT, heavy atom transfer, and other reactions, relative to predictions made by standard semi-local DFT alone.[251] This behavior is due to the elimination of the imbalance in density-driven errors between TSes and reactants.[251]

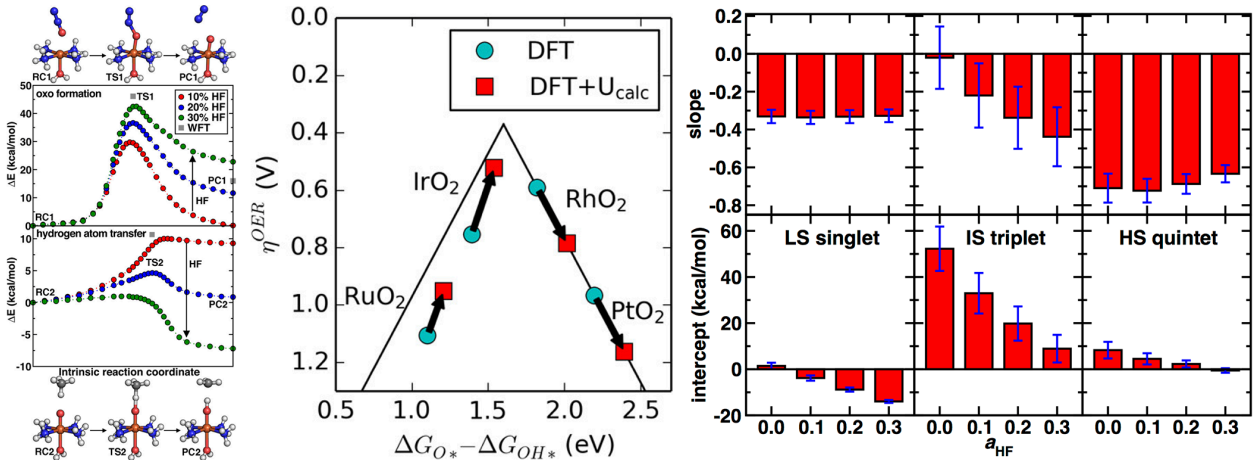


**Figure 15.** (left) Energy profiles of the oxo formation (top) and hydrogen atom transfer (bottom) reaction steps computed at 10% (red circles), 20% (blue circles), and 30% (green circles) HF exchange from ref 252. Structures of the reacting complex (RC), transition state (TS), and product complex (PC) corresponding to points indicated on the plots are provided at the top or bottom of each plot. The gray squares represent WFT reference energies, as described in the main text (DLPNO-CCSD(T)/CBS for oxo formation and NEVPT2(14,14)/def2-TZVPP for hydrogen atom transfer). Copyright 2017 American Chemical Society. (center) Predicted activity trends of 4*d* and 5*d* rutile dioxides calculated without (blue circle) and with (red square) the linear response *U* from ref 255. Arrows point in the direction that results from applying the linear response *U*. The volcano is fit to the idealized scaling relationships determined in a previous paper.[256] Copyright 2015 American Chemical Society. (right) Δ*E*(oxo) vs. Δ*E*(HAT) LFER slopes (top) and intercepts in kcal/mol (bottom) with standard errors (shown in blue) obtained across LS (left), IS (middle), and HS (right) Fe(II) resting state catalysts as a function of HF exchange fraction, $a_{HF}$, from ref 178. Zero-axes are shown by black solid lines. Copyright 2022

Springer Nature.

Despite widespread use in DFT carried out with local basis sets, hybrid calculations with an admixture of HF exchange are cost-prohibitive in solid-state systems, where low-cost DFT+U is preferred.[255-257] Prior studies[258-260] found that scaling relations (e.g. LFERs and BEPs) are less sensitive to DFA choice than property predictions. However, changing parameters (e.g., the Hubbard U in DFT+U calculations) can alter relative ranking of catalysts[255] (Figure 15). Furthermore, a recent study on partial methane oxidation by Vennelakanti *et al*. found that functional choice can alter relative reaction energetics and whether a reaction is spin-allowed[178] (Figure 15). For the catalysts in this work, increased HF exchange fractions make HAT more favorable while worsening oxo formation energetics[178] (Figure 15). Increased HF exchange systematically stabilizes HS states for all reactive intermediates, thus leading to predictions of a greater number of catalysts with spin-allowed reactivity with increasing exchange fractions.[178]

*5.3 Multi-reference (MR) Character and Method Accuracy*

Due to the high cost of correlated wavefunction theory calculations, DFT is widely used to study TMCs, despite being plagued with one-electron self-interaction and delocalization errors[261-262]. A study of HAT from methane by Fe(IV)-oxo moieties in triplet and quintet states shows comparable barrier height differences for both spin states between hybrid density functional (i.e., B3LYP) and restricted open-shell coupled cluster (RCCSD(T)) calculations.[263] Other studies[252, 264-265], however, have found that DFT predicts binding energies and reaction energies that differ from coupled cluster results by 10 kcal/mol, leading to incorrect predictions of reaction products, and have proposed alternate methods to evaluate TMC energetics (Figure 15).

While correlated wavefunction theory calculations of minimal model TMCs, such as those inspired by non-heme Fe-oxo intermediates, are frequently used to benchmark DFT calculations, canonical coupled cluster is computationally prohibitive for larger molecules[7]. Local coupled cluster methods exploit the fact that electron correlation is primarily short-range. They treat strong pairs of localized molecular orbitals at the highest level of theory, i.e., coupled cluster singles doubles and perturbative triples (CCSD(T)) while weak pairs are treated at lower levels of theory (e.g., MP2).[266] Two such local methods for studying larger molecules are local unrestricted CCSD(T0) (LUCCSD(T0)) and domain-based local pair natural orbital (DLPNO-CCSD(T)).[267-268] Limitations in local coupled cluster methods for practical systems (e.g. non-heme iron complexes) are primarily attributed to the breakdown of the domain and pair approximations.[267-268] Bioinspired synthetic non-heme iron complexes that carry out C–H activation are known to exhibit two-state reactivity[269-270], motivating studies of quintet–triplet energy gaps. A study of these gaps using LUCCSD(T0) and DLPNO-CCSD(T) revealed that the former systematically stabilizes low-spin states while the latter stabilizes high-spin states.[268] The pair error that leads to this imbalance in spin state energies, however, is reduced by using a "hotspot" approach that selectively includes key pairs at the CC level of theory.[4]

The most appropriate multi-reference method (i.e., that which has the best cost/accuracy tradeoff) for TMCs that contain too much multireference character to be treated by CCSD(T) is complete active space perturbation theory (CASPT2), despite its well-known bias in favor of HS states.[271] This bias is attributed to an inappropriate description of the metal (3s, 3p) correlation, which leads to inaccurate spin-state energetics.[271] To remove this bias, an alternative approach has been proposed, wherein metal (3s, 3p) correlation is estimated by CCSD or CCSD(T) depending on system size while the valence correlation is evaluated using CASPT2.[272] This bias-

eliminated approach has been used to characterize and compare HAT and epoxidation reaction pathways by an Fe(IV)-oxo intermediate, where both DFT and local coupled cluster methods perform poorly.[265] In more complex cases, where the description of the reference wave function requires two or more configuration state functions with comparable weights (e.g. systems with multireference character), single-reference methods (e.g. ROHF-CCSD, or the CC part of the CASPT2/CC approach) are expected to fail.[272] Thus, methods capable of accurately predicting properties of realistic catalysts remain an active area of research.

*5.4 Non-covalent Interactions (NCIs)*

Hydrogen bonds (HBs) are among the strongest NCIs, and include X–H···X[273] (X = N, O, F) and weaker C–H···O[274] interactions. HBs consist of a strong electrostatic component and partial covalent bond formation, which gives rise to their directional nature.[275-276] HBs are prevalent in nature and play a crucial role in governing enzyme selectivity.[277] Predicting NCIs accurately, however, is difficult for both force fields[278-281], due to functional form limitations, and DFT, even with the inclusion of dispersion corrections[282-284] (Figure 16). Studies by Qi *et al*.[279] and Zhou *et al*.[285] showed that shorter HB distances that are characterized as unfavorable by force fields consist of favorable HB interactions (Figure 16). Studies with more accurate wavefunction theory calculations[278, 286] including DLPNO-CCSD(T) revealed that the commonly observed NCIs in proteins are predicted accurately using model systems and wavefunction theory methods (Figure 16).

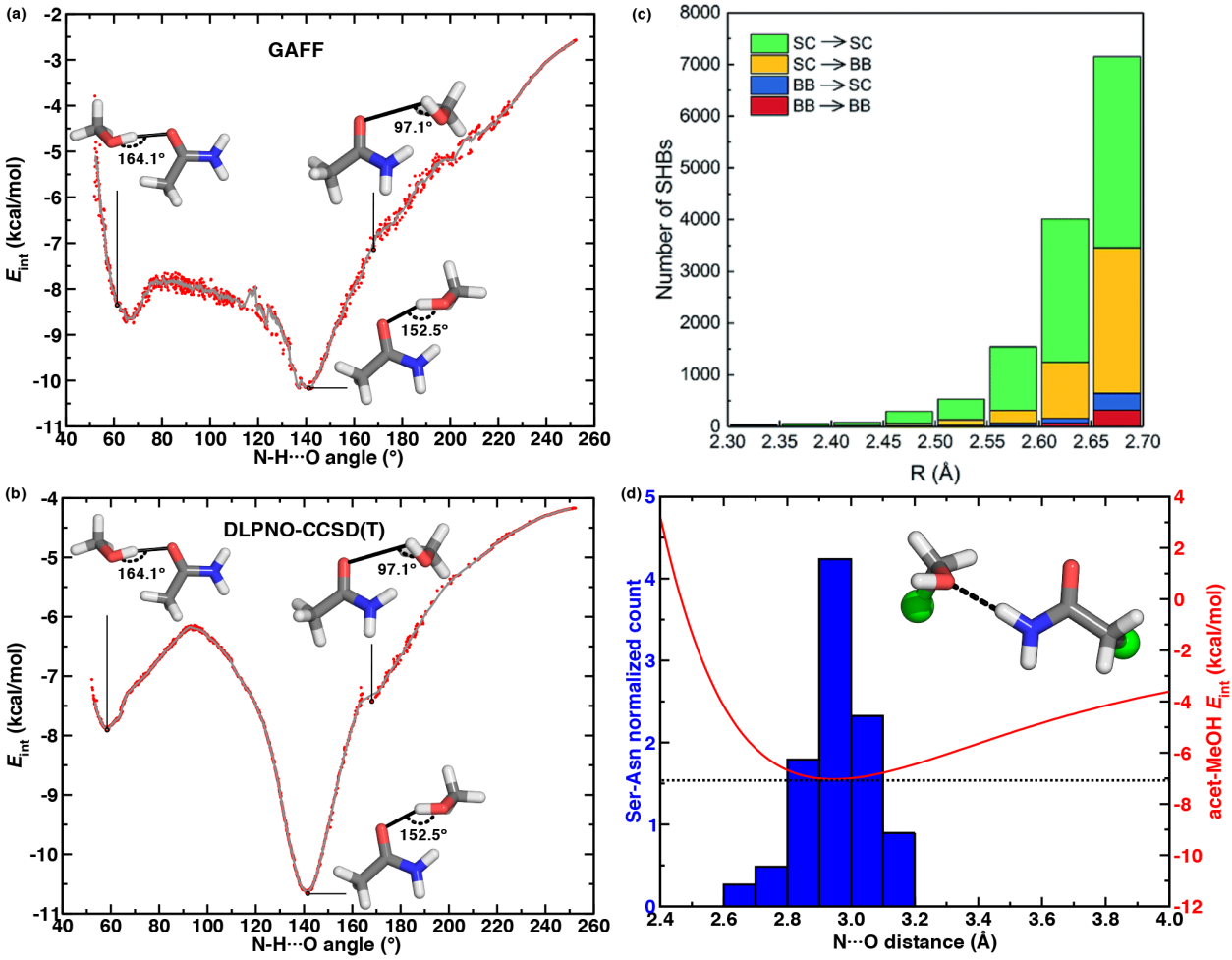


**Figure 16.** Reaction coordinate for interconversion from an O–H···O HB to an ambifunctional HB and to an N–H···O HB in a model system of Ser/Thr–Asn/Gln with (a) GAFF and (b) DLPNO-CCSD(T), from ref. 278. Copyright 2021 Royal Society of Chemistry. (c) Stacked histogram (0.05 Å bin width) of shortest heavy-atom distances in HBs grouped by backbone (BB) or sidechain (SC) interaction type from ref. 285. Copyright 2019 Royal Society of Chemistry. (d) Normalized histograms (blue, left axes) of heavy-atom HB distances (bin width of 0.1 Å) for Ser–Asn N–H···O HBs X-ray crystal structures with the one-dimensional potential energy curves (red, right axes) for acetamide–methanol overlaid, from ref 278. Copyright 2021 Royal Society of Chemistry.

NCIs between the reacting substrate and the greater catalyst structure have been shown to be important in the radical rebound mechanism. For example, NCIs on model synthetic complexes influence whether HAT occurs to the Fe(IV)-oxo moiety or to a distinct ligand in the complex.[287] In turn, the NCIs influence both the identity of the reactive intermediates and the

reaction mechanism.[287] A computational study by Mehmood *et al*. found that simultaneous HBs between the substrate and amino-acid backbone influence substrate positioning in SyrB2 and dictate the enzyme selectivity for halogenation.[12] An experimental study by Mitchell *et al*. proposed that an HB interaction of Ser with the Fe(IV)-oxo moiety in the WelO5 enzyme promotes selective halogenation.[13] To mimic these patterns frequently observed in enzymes, ligands in synthetic complexes have been designed with functional groups installed to promote NCIs, where the number and type of HBs affect reactivity.[157, 288] The installation of functional groups proximal to the Fe(IV)-oxo moiety that has worked for molecules has also been demonstrated in MOFs.[248] In these systems, the NCIs weaken the metal-oxo bond strength and subsequently lower the activation barrier for HAT.[157, 248, 289]

*5.5 Machine Learning (ML) for Chemical Discovery*

ML has started to address combinatorial challenges in chemical discovery for catalysis.[290-293] Schneider *et al*. used statistical analysis and observed that PCET thermodynamics can predict barrier heights over a set of diverse metal-oxo complexes[159], reproducing computational observations of a universal HAT BEP relationship.[236-237] When these linear QM-descriptor relations do not hold across metals, oxidation states, and spin states[129, 158] or the QM descriptor is expensive to compute[294-295], ML provides a general path forward for design. Using ML, Nandy *et al*. discovered a class of catalysts that are oxidatively stable in their resting states but still form metal-oxo moieties favorably.[158] These compounds are missed by linear QM-descriptor-based relations that assume that compounds are either oxidatively stable or form metal-oxo moieties favorably, but not both.[158, 240] Nandy *et al*. also recently trained artificial neural network (ANN) models that map catalyst connectivity to reaction energies and used ANN-driven efficient global optimization (EGO) with a two-dimensional expected

improvement[296] (2D-EI) criterion to design catalysts that could simultaneously activate methane but release methanol[129] (Figure 9). Their search over 16M compounds could be done with ML in minutes but would take decades with full DFT evaluation. Simultaneously, optimization over this chemical space took advantage of broken scaling relations to design catalysts that have improved methane oxidation thermodynamics.

ML-driven HTVS of bioinspired catalysts has the potential to uncover synthetic catalysts that are more stable, active, and selective than their metalloenzyme counterparts.[18, 297] Current catalyst design studies, however, assume a reaction cycle, which may bias conclusions on the optimal catalyst design.[166, 192] Duan *et al*. recently developed transferable workflows to predict calculation outcomes relevant to catalysis that can accelerate the reaction intermediate screening for mechanism elucidation.[298-299] Beyond reaction intermediates, TS structures are challenging to converge. Therefore, ML can accelerate the prediction of guessed TS geometries to avoid expensive TS searches by DFT.[300]

For heterogeneous single-site catalysts, challenges with representations[184, 301-302] and data availability have limited the widespread use of ML for catalyst screening.[303] Instead, experimental data has been leveraged to identify catalysts that are thermally stable and usable for catalysis.[200] Similarly, ML trained on experimental data has been used to assign oxidation states to metal ions in MOFs based on their metal-local chemical environment.[304] As data sets grow in size and fidelity, ML be increasingly used for bioinspired catalyst design as it is applied to zeolite, MOF, and SAC high-throughput screening.

**6. Conclusions and Outlook.**

The challenge of activating inert C–H bonds has motivated the study of catalysts to draw from what can be accomplished with natural enzymes and translate these advantageous features

into TMC and material mimics. Inert C–H bond activation reactivity has been observed in a diverse number of iron-containing enzymes from the heme-P450s to non-heme iron α-ketoglutarate-dependent enzymes and methane monooxygenases. Computational studies have played a key role in quantifying the effect of the active site environment on reaction energetics, understanding the role of metal, oxidation, and spin state in reactivity, confirming spectroscopic assignments, and investigating substrate positioning and its influence on reactivity. All of these insights have brought about new hypotheses that have led to catalyst design for improved C–H bond reactivity.

Bioinspired efforts aiming to recreate the primary coordination sphere of metalloenzymes have focused on TMC ligand design. Here, computational studies have unraveled the effects of various coordination environments, oxidation, and spin states on metal–ligand binding and C–H bond reactivity. This in turn has led to new hypotheses and ligand design improvements. As ligand designs have evolved, DFT has been essential in quantifying the differences between TMCs that have the same ground state spin and comparable spectroscopic observables but distinct reactivity.

Bioinspired catalyst design efforts have also motivated the installation of single metal active sites in heterogeneous catalysts such as zeolites, MOFs, and SACs, making the catalyst readily separable from reactants and products. Because the complex chemical environments challenge the spectroscopic characterization of the catalytically active species, DFT has proven essential in studying these intermediates that are difficult to experimentally characterize with atomic precision. In addition to aiding spectroscopic assignments, computational studies have played an essential role in decoupling the effects of through-bond and through-space interactions in these materials.

While computation has played a critical role in understanding routes to selective C–H activation, numerous outstanding challenges remain. DFT is often the method of choice for studying catalyst reaction pathways in both biological and non-biological systems thanks to its favorable cost–accuracy trade-off. Nevertheless, the well-localized *d*-electrons in many cases necessitate beyond-DFT wavefunction theory calculations for accurate prediction of molecular properties. Scaling relations (i.e., BEP relations or LFERs) derived from DFT-calculated energetics are often used to accelerate screening of bulk metals for heterogeneous catalysis, but their applicability is far more limited in TMCs or single-site heterogeneous catalysts. Catalyst properties may also be governed by subtle energy differences such as those cause by the presence of NCIs, which are challenging to accurately model with DFT or classical force fields. ML models present one path to addressing the combinatorial challenge of catalyst design, but it remains unclear how to address inheritance by the ML model of the biases in the underlying training data.

As we learn more about how metalloprotein active sites catalyze C–H bond activation, we gain more information to design synthetic bioinspired catalysts. ML can help encapsulate this information to accelerate ligand design, where there are too many possibilities to consider for an exhaustive DFT screen. ML can also make higher-cost methods more tractable for high-throughput screening through corrective schemes. Harnessing a deep computationally guided understanding of metalloprotein active sites and bioinspired catalysts will lead to the design of stable, active, and selective catalysts that provide industrially viable solutions for outstanding "holy grail" challenges such as selective C–H activation of methane.

AUTHOR INFORMATION

**Corresponding Author**

*email:hjkulik@mit.edu

**Notes**

The authors declare no competing financial interest.

ACKNOWLEDGMENT

This work was supported by the National Science Foundation grant numbers CBET-1704266 and CBET-1846426; the United States Department of Energy grant numbers DE-SC0012702 and DE-SC0018096; DARPA grant number D18AP00039; the Office of Naval Research grant numbers N00014-17-1-2956, N00014-18-1-2434, and N00014-20-1-2150; a National Science Foundation Graduate Research Fellowship under Grant #1122374 (to A.N.) and #1745302 (to D.W.K.); an AAAS Marion Milligan Mason Award; an Alfred P. Sloan Fellowship in Chemistry; and a Burroughs-Wellcome Fund Career Award at the Scientific Interface. The authors thank Adam H. Steeves for providing a critical reading of the manuscript.

REFERENCES


1. Olah, G. A., Beyond Oil and Gas: The Methanol Economy. *Angew. Chem. Int. Ed.* **2005,** *44* (18), 2636-2639.
2. Lunsford, J. H., Catalytic Conversion of Methane to More Useful Chemicals and Fuels: a Challenge for the 21st Century. *Catal. Today* **2000,** *63* (2-4), 165-174.
3. Galonić Fujimori, D.; Barr, E. W.; Matthews, M. L.; Koch, G. M.; Yonce, J. R.; Walsh, C. T.; Bollinger, J. M.; Krebs, C.; Riggs-Gelasco, P. J., Spectroscopic Evidence for a High-Spin Br-Fe(IV)-Oxo Intermediate in the α-Ketoglutarate-Dependent Halogenase CytC3 from Streptomyces. *J. Am. Chem. Soc.* **2007,** *129* (44), 13408-13409.
4. Krebs, C.; Galonić Fujimori, D.; Walsh, C. T.; Bollinger, J. M., Non-Heme Fe(IV)–Oxo Intermediates. *Acc. Chem. Res.* **2007,** *40* (7), 484-492.
5. Wong, S. D.; Srnec, M.; Matthews, M. L.; Liu, L. V.; Kwak, Y.; Park, K.; Bell, C. B.; Alp, E. E.; Zhao, J. Y.; Yoda, Y.; Kitao, S.; Seto, M.; Krebs, C.; Bollinger, J. M., Jr.; Solomon, E. I., Elucidation of the Fe(IV)=O Intermediate in the Catalytic Cycle of the Halogenase SyrB2. *Nature* **2013,** *499* (7458), 320-323.
6. Wang, V. C. C.; Maji, S.; Chen, P. P. Y.; Lee, H. K.; Yu, S. S. F.; Chan, S. I., Alkane Oxidation: Methane Monooxygenases, Related Enzymes, and Their Biomimetics. *Chem. Rev.* **2017,** *117* (13), 8574-8621.
7. Price, J. C.; Barr, E. W.; Tirupati, B.; Bollinger, J. M.; Krebs, C., The First Direct Characterization of a High-Valent Iron Intermediate in the Reaction of an α-Ketoglutarate-Dependent Dioxygenase: A High-Spin Fe(IV) Complex in Taurine/α-Ketoglutarate Dioxygenase (TauD) from Escherichia Coli. *Biochemistry* **2003,** *42* (24), 7497-7508.
8. Sinnecker, S.; Svensen, N.; Barr, E. W.; Ye, S.; Bollinger, J. M.; Neese, F.; Krebs, C., Spectroscopic and Computational Evaluation of the Structure of the High-Spin Fe(IV)-Oxo Intermediates in Taurine: α-Ketoglutarate Dioxygenase from Escherichia coli and Its His99Ala Ligand Variant. *J. Am. Chem. Soc.* **2007,** *129* (19), 6168-6179.
9. Krebs, C.; Price, J. C.; Baldwin, J.; Saleh, L.; Green, M. T.; Bollinger, J. M., Rapid Freeze-Quench $^{57}$Fe Mössbauer Spectroscopy: Monitoring Changes of an Iron-Containing Active Site During a Biochemical Reaction. *Inorg. Chem.* **2005,** *44* (4), 742-757.
10. Snyder, B. E. R.; Bols, M. L.; Schoonheydt, R. A.; Sels, B. F.; Solomon, E. I., Iron and Copper Active Sites in Zeolites and Their Correlation to Metalloenzymes. *Chem. Rev.* **2018,** *118* (5), 2718-2768.
11. England, J.; Martinho, M.; Farquhar, E. R.; Frisch, J. R.; Bominaar, E. L.; Munck, E.; Que, L., Jr., A Synthetic High-Spin Oxoiron(IV) Complex: Generation, Spectroscopic Characterization, and Reactivity. *Angew. Chem. Int. Ed.* **2009,** *48* (20), 3622-3626.
12. Kaizer, J.; Klinker, E. J.; Oh, N. Y.; Rohde, J.-U.; Song, W. J.; Stubna, A.; Kim, J.; Münck, E.; Nam, W.; Que, L., Nonheme $Fe^{IV}O$ Complexes That Can Oxidize the C–H Bonds of Cyclohexane at Room Temperature. *J. Am. Chem. Soc.* **2003,** *126* (2), 472-473.
13. Biswas, A. N.; Puri, M.; Meier, K. K.; Oloo, W. N.; Rohde, G. T.; Bominaar, E. L.; Münck, E.; Que, L., Modeling TauD-J: A High-Spin Nonheme Oxoiron(IV) Complex with High Reactivity Toward C–H Bonds. *J. Am. Chem. Soc.* **2015,** *137* (7), 2428-2431.
14. Rohde, J.-U.; In, J.-H.; Lim, M. H.; Brennessel, W. W.; Bukowski, M. R.; Stubna, A.; Münck, E.; Nam, W.; Que, L., Crystallographic and Spectroscopic Characterization of a Nonheme Fe(IV)=O Complex. *Science* **2003,** *299* (5609), 1037-1039.

15. Pestovsky, O.; Stoian, S.; Bominaar, E. L.; Shan, X.; Münck, E.; Que, L.; Bakac, A., Aqueous $Fe^{IV}$=O: Spectroscopic Identification and Oxo-Group Exchange. *Angew. Chem. Int. Ed.* **2005,** *44* (42), 6871-6874.
16. Grapperhaus, C. A.; Mienert, B.; Bill, E.; Weyhermüller, T.; Wieghardt, K., Mononuclear (Nitrido)iron(V) and (Oxo)iron(IV) Complexes via Photolysis of $[(cyclam\text{-}acetato)Fe^{III}(N_3)]^+$ and Ozonolysis of $[(cyclam\text{-}acetato)Fe^{III}(O_3SCF_3)]^+$ in Water/Acetone Mixtures. *Inorg. Chem.* **2000,** *39* (23), 5306-5317.
17. Thiel, W., Computational Catalysis-Past, Present, and Future. *Angew. Chem. Int. Ed.* **2014,** *53* (33), 8605-8613.
18. Foscato, M.; Jensen, V. R., Automated in Silico Design of Homogeneous Catalysts. *ACS Catal.* **2020,** *10* (3), 2354-2377.
19. Klein, J. E. M. N.; Knizia, G., cPCET versus HAT: A Direct Theoretical Method for Distinguishing X-H Bond-Activation Mechanisms. *Angew. Chem. Int. Ed.* **2018,** *57* (37), 11913-11917.
20. Ye, S.; Geng, C.-Y.; Shaik, S.; Neese, F., Electronic Structure Analysis of Multistate Reactivity in Transition Metal Catalyzed Reactions: the Case of C–H Bond Activation by Non-Heme Iron(IV)–Oxo Cores. *Phys. Chem. Chem. Phys.* **2013,** *15* (21), 8017.
21. Yadav, V.; Gordon, J. B.; Siegler, M. A.; Goldberg, D. P., Dioxygen-Derived Nonheme Mononuclear $Fe^{III}$(OH) Complex and Its Reactivity with Carbon Radicals. *J. Am. Chem. Soc.* **2019,** *141* (26), 10148-10153.
22. Yadav, V.; Rodriguez, R. J.; Siegler, M. A.; Goldberg, D. P., Determining the Inherent Selectivity for Carbon Radical Hydroxylation versus Halogenation with $Fe^{III}$(OH)(X) Complexes: Relevance to the Rebound Step in Non-heme Iron Halogenases. *J. Am. Chem. Soc.* **2020,** *142* (16), 7259-7264.
23. Rosen, A. S.; Notestein, J. M.; Snurr, R. Q., Structure–Activity Relationships That Identify Metal–Organic Framework Catalysts for Methane Activation. *ACS Catal.* **2019,** *9* (4), 3576-3587.
24. Jia, H. J.; Nandy, A.; Liu, M. J.; Kulik, H. J., Modeling the Roles of Rigidity and Dopants in Single-Atom Methane-to-Methanol Catalysts. *J. Mater. Chem. A* **2022,** *10*, 6193-6203.
25. Groves, J. T.; McClusky, G. A., Aliphatic Hydroxylation via Oxygen Rebound. Oxygen Transfer Catalyzed by Iron. *J. Am. Chem. Soc.* **1976,** *98* (3), 859-861.
26. Groves, J. T., Key Elements of the Chemistry of Cytochrome P-450: The Oxygen Rebound Mechanism. *J. Chem. Ed.* **1985,** *62* (11), 928-931.
27. Hager, L. P.; Doubek, D. L.; Silverstein, R. M.; Hargis, J. H.; Martin, J. C., Chloroperoxidase. IX. Structure of Compound I. *J. Am. Chem. Soc.* **1972,** *94* (12), 4364-4366.
28. Denisov, I. G.; Makris, T. M.; Sligar, S. G.; Schlichting, I., Structure and Chemistry of Cytochrome P450. *Chem. Rev.* **2005,** *105* (6), 2253-2278.
29. Huang, X.; Groves, J. T., Oxygen Activation and Radical Transformations in Heme Proteins and Metalloporphyrins. *Chem. Rev.* **2017,** *118* (5), 2491-2553.
30. Kumar, D.; de Visser, S. P.; Sharma, P. K.; Cohen, S.; Shaik, S., Radical Clock Substrates, Their C–H Hydroxylation Mechanism by Cytochrome P450, and Other Reactivity Patterns: What Does Theory Reveal about the Clocks' Behavior? *J. Am. Chem. Soc.* **2004,** *126* (6), 1907-1920.
31. Renata, H.; Lewis, R. D.; Sweredoski, M. J.; Moradian, A.; Hess, S.; Wang, Z. J.; Arnold, F. H., Identification of Mechanism-Based Inactivation in P450-Catalyzed

Cyclopropanation Facilitates Engineering of Improved Enzymes. *J. Am. Chem. Soc.* **2016,** *138* (38), 12527-12533.
32. Shaik, S.; Kumar, D.; de Visser, S. P.; Altun, A.; Thiel, W., Theoretical Perspective on the Structure and Mechanism of Cytochrome P450 Enzymes. *Chem. Rev.* **2005,** *105* (6), 2279-2328.
33. Meunier, B.; de Visser, S. P.; Shaik, S., Mechanism of Oxidation Reactions Catalyzed by Cytochrome P450 Enzymes. *Chem. Rev.* **2004,** *104* (9), 3947-3980.
34. Ogliaro, F.; Harris, N.; Cohen, S.; Filatov, M.; de Visser, S. P.; Shaik, S., A Model "Rebound" Mechanism of Hydroxylation by Cytochrome P450: Stepwise and Effectively Concerted Pathways, and Their Reactivity Patterns. *J. Am. Chem. Soc.* **2000,** *122* (37), 8977-8989.
35. de Visser, S. P.; Ogliaro, F.; Sharma, P. K.; Shaik, S., What Factors Affect the Regioselectivity of Oxidation by Cytochrome P450? A DFT Study of Allylic Hydroxylation and Double Bond Epoxidation in a Model Reaction. *J. Am. Chem. Soc.* **2002,** *124* (39), 11809-11826.
36. Ogliaro, F.; Cohen, S.; de Visser, S. P.; Shaik, S., Medium Polarization and Hydrogen Bonding Effects on Compound I of Cytochrome P450: What Kind of a Radical Is It Really? *J. Am. Chem. Soc.* **2000,** *122* (51), 12892-12893.
37. Guallar, V.; Baik, M.-H.; Lippard, S. J.; Friesner, R. A., Peripheral Heme Substituents Control the Hydrogen-Atom Abstraction Chemistry in Cytochromes P450. *Proc. Natl. Acad. Sci. U.S.A.* **2003,** *100* (12), 6998-7002.
38. Acevedo-Rocha, C. G.; Li, A.; D'Amore, L.; Hoebenreich, S.; Sanchis, J.; Lubrano, P.; Ferla, M. P.; Garcia-Borràs, M.; Osuna, S.; Reetz, M. T., Pervasive Cooperative Mutational Effects on Multiple Catalytic Enzyme Traits Emerge via Long-Range Conformational Dynamics. *Nat. Commun.* **2021,** *12*, 1521.
39. Bím, D.; Alexandrova, A. N., Local Electric Fields As a Natural Switch of Heme-Iron Protein Reactivity. *ACS Catal.* **2021,** *11* (11), 6534-6546.
40. Coelho, P. S.; Brustad, E. M.; Kannan, A.; Arnold, F. H., Olefin Cyclopropanation via Carbene Transfer Catalyzed by Engineered Cytochrome P450 Enzymes. *Science* **2013,** *339* (6117), 307-310.
41. Dodani, S. C.; Kiss, G.; Cahn, J. K. B.; Su, Y.; Pande, V. S.; Arnold, F. H., Discovery of a Regioselectivity Switch in Nitrating P450s Guided by Molecular Dynamics Simulations and Markov Models. *Nat. Chem.* **2016,** *8* (5), 419-425.
42. Herr, C. Q.; Hausinger, R. P., Amazing Diversity in Biochemical Roles of Fe(II)/2-Oxoglutarate Oxygenases. *Trends Biochem. Sci.* **2018,** *43* (7), 517-532.
43. Islam, M. S.; Leissing, T. M.; Chowdhury, R.; Hopkinson, R. J.; Schofield, C. J., 2-Oxoglutarate-Dependent Oxygenases. *Annu. Rev. Biochem.* **2018,** *87* (1), 585-620.
44. Smith, J. L.; Khare, D., Recent Advances in the Structural and Mechanistic Biology of Non-Haem Fe(II), 2-Oxoglutarate and $O_2$-Dependent Halogenases. In *2-Oxoglutarate-Dependent Oxygenases*, The Royal Society of Chemistry: 2015; pp 401-413.
45. Price, J. C.; Barr, E. W.; Glass, T. E.; Krebs, C.; Bollinger, J. M., Evidence for Hydrogen Abstraction from C1 of Taurine by the High-Spin Fe(IV) Intermediate Detected During Oxygen Activation by Taurine:α-Ketoglutarate Dioxygenase (TauD). *J. Am. Chem. Soc.* **2003,** *125* (43), 13008-13009.
46. Wojdyla, Z.; Borowski, T., Properties of the Reactants and Their Interactions Within and With the Enzyme Binding Cavity Determine Reaction Selectivities. The Case of Fe(II)/2-Oxoglutarate Dependent Enzymes. *Chem. Eur. J.* **2022,** *28* (18), e202104106.

47. Mehmood, R.; Qi, H. W.; Steeves, A. H.; Kulik, H. J., The Protein's Role in Substrate Positioning and Reactivity for Biosynthetic Enzyme Complexes: The Case of SyrB2/SyrB1. *ACS Catal.* **2019,** *9* (6), 4930-4943.
48. de Visser, S. P., Second-Coordination Sphere Effects on Selectivity and Specificity of Heme and Nonheme Iron Enzymes. *Chem. Eur. J.* **2020,** *26* (24), 5308-5327.
49. Kulik, H. J.; Drennan, C. L., Substrate Placement Influences Reactivity in Non-heme Fe(II) Halogenases and Hydroxylases. *J. Biol. Chem.* **2013,** *288* (16), 11233-11241.
50. Vaillancourt, F. H.; Yin, J.; Walsh, C. T., SyrB2 in Syringomycin E Biosynthesis is a Nonheme $Fe^{II}$ α-ketoglutarate- and $O_2$-dependent Halogenase. *Proc. Natl. Acad. Sci. U.S.A.* **2005,** *102* (29), 10111-10116.
51. Wang, B.; Cao, Z.; Rovira, C.; Song, J.; Shaik, S., Fenton-Derived OH Radicals Enable the MPnS Enzyme to Convert 2-Hydroxyethylphosphonate to Methylphosphonate: Insights from Ab Initio QM/MM MD Simulations. *J. Am. Chem. Soc.* **2019,** *141* (23), 9284-9291.
52. Del Rio Flores, A.; Kastner, D. W.; Du, Y.; Narayanamoorthy, M.; Shen, Y.; Cai, W.; Vennelakanti, V.; Zill, N. A.; Dell, L. B.; Zhai, R.; Kulik, H. J.; Zhang, W., Probing the Mechanism of Isonitrile Formation by a Non-Heme Iron(II)-Dependent Oxidase/Decarboxylase. *J. Am. Chem. Soc.* **2022,** *144* (13), 5893-5901.
53. Chen, T.-Y.; Zheng, Z.; Zhang, X.; Chen, J.; Cha, L.; Tang, Y.; Guo, Y.; Zhou, J.; Wang, B.; Liu, H.-w.; Chang, W.-c., Deciphering the Reaction Pathway of Mononuclear Iron Enzyme-Catalyzed N≡C Triple Bond Formation in Isocyanide Lipopeptide and Polyketide Biosynthesis. *ACS Catal.* **2022,** *12* (4), 2270-2279.
54. Ali, H. S.; Henchman, R. H.; Warwicker, J.; de Visser, S. P., How Do Electrostatic Perturbations of the Protein Affect the Bifurcation Pathways of Substrate Hydroxylation Versus Desaturation in the Nonheme Iron-Dependent Viomycin Biosynthesis Enzyme? *J. Phys. Chem. A* **2021,** *125* (8), 1720-1737.
55. Nakashima, Y.; Mori, T.; Nakamura, H.; Awakawa, T.; Hoshino, S.; Senda, M.; Senda, T.; Abe, I., Structure Function and Engineering of Multifunctional Non-Heme Iron Dependent Oxygenases in Fungal Meroterpenoid Biosynthesis. *Nat. Commun.* **2018,** *9* (1), 104.
56. Martinie, R. J.; Livada, J.; Chang, W.-c.; Green, M. T.; Krebs, C.; Bollinger, J. M.; Silakov, A., Experimental Correlation of Substrate Position with Reaction Outcome in the Aliphatic Halogenase, SyrB2. *J. Am. Chem. Soc.* **2015,** *137* (21), 6912-6919.
57. Srnec, M.; Solomon, E. I., Frontier Molecular Orbital Contributions to Chlorination Versus Hydroxylation Selectivity in the Non-Heme Iron Halogenase SyrB2. *J. Am. Chem. Soc.* **2017,** *139* (6), 2396-2407.
58. Weichold, V.; Milbredt, D.; van Pée, K.-H., Specific Enzymatic Halogenation—From the Discovery of Halogenated Enzymes to Their Applications In Vitro and In Vivo. *Angew. Chem. Int. Ed.* **2016,** *55* (22), 6374-6389.
59. Huang, J.; Li, C.; Wang, B.; Sharon, D. A.; Wu, W.; Shaik, S., Selective Chlorination of Substrates by the Halogenase SyrB2 is Controlled by the Protein According to a Combined Quantum Mechanics/Molecular Mechanics and Molecular Dynamics Study. *ACS Catal.* **2016,** *6* (4), 2694-2704.
60. Borowski, T.; Noack, H.; Radon, M.; Zych, K.; Siegbahn, P. E., Mechanism of Selective Halogenation by SyrB2: a Computational Study. *J. Am. Chem. Soc.* **2010,** *132* (37), 12887-98.
61. Mehmood, R.; Vennelakanti, V.; Kulik, H. J., Spectroscopically Guided Simulations Reveal Distinct Strategies for Positioning Substrates to Achieve Selectivity in Nonheme Fe(II)/α-Ketoglutarate-Dependent Halogenases. *ACS Catal.* **2021,** *11* (19), 12394-12408.

62. Zhang, X.; Wang, Z.; Gao, J.; Liu, W., Chlorination Versus Hydroxylation Selectivity Mediated by the Non-Heme Iron Halogenase WelO5. *Phys. Chem. Chem. Phys.* **2020,** *22* (16), 8699-8712.
63. Neugebauer, M. E.; Sumida, K. H.; Pelton, J. G.; McMurry, J. L.; Marchand, J. A.; Chang, M. C. Y., A Family of Radical Halogenases for the Engineering of Amino-Acid-Based Products. *Nat. Chem. Biol.* **2019,** *15* (10), 1009-1016.
64. Ali, H. S.; Ghafoor, S.; de Visser, S. P., Density Functional Theory Study into the Reaction Mechanism of Isonitrile Biosynthesis by the Nonheme Iron Enzyme ScoE. *Top. Catal.* **2022,** *65*, 528-543.
65. Li, H.; Liu, Y., Mechanistic Investigation of Isonitrile Formation Catalyzed by the Nonheme Iron/α-KG-dependent Decarboxylase (ScoE). *ACS Catal.* **2020,** *10* (5), 2942-2957.
66. Chen, T. Y.; Chen, J. F.; Tang, Y. J.; Zhou, J. H.; Guo, Y. S.; Chang, W. C., Pathway from N-Alkylglycine to Alkylisonitrile Catalyzed by Iron(II) and 2-Oxoglutarate-Dependent Oxygenases. *Angew. Chem. Int. Ed.* **2020,** *59* (19), 7367-7371.
67. Borowski, T.; Bassan, A.; Siegbahn, P. E. M., Mechanism of Dioxygen Activation in 2-Oxoglutarate-Dependent Enzymes: A Hybrid DFT Study. *Chem. Eur. J.* **2004,** *10* (4), 1031-1041.
68. Ali, H. S.; Henchman, R. H.; de Visser, S. P., What Determines the Selectivity of Arginine Dihydroxylation by the Nonheme Iron Enzyme OrfP? *Chem. Eur. J.* **2021,** *27* (5), 1795-1809.
69. Dunham, N. P.; Chang, W.-c.; Mitchell, A. J.; Martinie, R. J.; Zhang, B.; Bergman, J. A.; Rajakovich, L. J.; Wang, B.; Silakov, A.; Krebs, C.; Boal, A. K.; Bollinger, J. M., Two distinct mechanisms for C–C desaturation by iron(II)- and 2-(oxo)glutarate-dependent oxygenases: Importance of α-heteroatom assistance. *J. Am. Chem. Soc.* **2018,** *140* (23), 7116-7126.
70. Martinez, S.; Fellner, M.; Herr, C. Q.; Ritchie, A.; Hu, J.; Hausinger, R. P., Structures and Mechanisms of the Non-Heme Fe(II)- and 2-Oxoglutarate-Dependent Ethylene-Forming Enzyme: Substrate Binding Creates a Twist. *J. Am. Chem. Soc.* **2017,** *139* (34), 11980-11988.
71. Chaturvedi, S. S.; Ramanan, R.; Hu, J.; Hausinger, R. P.; Christov, C. Z., Atomic and Electronic Structure Determinants Distinguish Between Ethylene Formation and L-arginine Hydroxylation Reaction Mechanisms in the Ethylene-Forming Enzyme. *ACS Catal.* **2021,** *11* (3), 1578-1592.
72. Xue, J.; Lu, J.; Lai, W., Mechanistic Insights into a Non-Heme 2-Oxoglutarate-Dependent Ethylene-Forming Enzyme: Selectivity of Ethylene-Formation Versus l-Arg Hydroxylation. *Phys. Chem. Chem. Phys.* **2019,** *21* (19), 9957-9968.
73. Tinberg, C. E.; Lippard, S. J., Dioxygen Activation in Soluble Methane Monooxygenase. *Acc. Chem. Res.* **2011,** *44* (4), 280-288.
74. Ross, M. O.; Rosenzweig, A. C., A Tale of Two Methane Monooxygenases. *J. Biol. Inorg. Chem.* **2017,** *22* (2), 307-319.
75. Rosenzweig, A. C.; Frederick, C. A.; Lippard, S. J.; Nordlund, P., Crystal Structure of a Bacterial Non-Haem Iron Hydroxylase that Catalyses the Biological Oxidation of Methane. *Nature* **1993,** *366* (6455), 537-543.
76. Cutsail, G. E.; Banerjee, R.; Zhou, A.; Que, L.; Lipscomb, J. D.; DeBeer, S., High-Resolution Extended X-ray Absorption Fine Structure Analysis Provides Evidence for a Longer Fe···Fe Distance in the Q Intermediate of Methane Monooxygenase. *J. Am. Chem. Soc.* **2018,** *140* (48), 16807-16820.

77. Gherman, B. F.; Lippard, S. J.; Friesner, R. A., Substrate Hydroxylation in Methane Monooxygenase: Quantitative Modeling via Mixed Quantum Mechanics/Molecular Mechanics Techniques. *J. Am. Chem. Soc.* **2005,** *127* (3), 1025-1037.
78. Fox, B. G.; Borneman, J. G.; Wackett, L. P.; Lipscomb, J. D., Haloalkene Oxidation by the Soluble Methane Monooxygenase from Methylosinus Trichosporium OB3b: Mechanistic and Environmental Implications. *Biochemistry* **1990,** *29* (27), 6419-6427.
79. Liu, K. E.; Johnson, C. C.; Newcomb, M.; Lippard, S. J., Radical Clock Substrate Probes and Kinetic Isotope Effect Studies of the Hydroxylation of Hydrocarbons by Methane Monooxygenase. *J. Am. Chem. Soc.* **1993,** *115* (3), 939-947.
80. Lee, S. K.; Nesheim, J. C.; Lipscomb, J. D., Transient intermediates of the methane monooxygenase catalytic cycle. *J. Biol. Chem.* **1993,** *268* (29), 21569-21577.
81. Shu, L.; Nesheim, J. C.; Kauffmann, K.; Münck, E.; Lipscomb, J. D.; Que, L., An $Fe_2^{IV}O_2$ Diamond Core Structure for the Key Intermediate Q of Methane Monooxygenase. *Science* **1997,** *275* (5299), 515-518.
82. Castillo, R. G.; Banerjee, R.; Allpress, C. J.; Rohde, G. T.; Bill, E.; Que, L.; Lipscomb, J. D.; DeBeer, S., High-Energy-Resolution Fluorescence-Detected X-ray Absorption of the Q Intermediate of Soluble Methane Monooxygenase. *J. Am. Chem. Soc.* **2017,** *139* (49), 18024-18033.
83. Schulz, C. E.; Castillo, R. G.; Pantazis, D. A.; DeBeer, S.; Neese, F., Structure–Spectroscopy Correlations for Intermediate Q of Soluble Methane Monooxygenase: Insights from QM/MM Calculations. *J. Am. Chem. Soc.* **2021,** *143* (17), 6560-6577.
84. Dunietz, B. D.; Beachy, M. D.; Cao, Y.; Whittington, D. A.; Lippard, S. J.; Friesner, R. A., Large Scale Ab Initio Quantum Chemical Calculation of the Intermediates in the Soluble Methane Monooxygenase Catalytic Cycle. *J. Am. Chem. Soc.* **2000,** *122* (12), 2828-2839.
85. Kloer, D. P.; Hagel, C.; Heider, J.; Schulz, G. E., Crystal Structure of Ethylbenzene Dehydrogenase from Aromatoleum Aromaticum. *Structure* **2006,** *14*, 1377–1388.
86. Heider, J.; Szaleniec, M.; Sünwoldt, K.; Boll, M., Ethylbenzene Dehydrogenase and Related Molybdenum Enzymes Involved in Oxygen Independent Alkyl Chain Hydroxylation. *J. Mol. Microbiol. Biotechnol.* **2016,** *26*, 45–62.
87. Hille, R.; Hall, J.; Basu, P., The Mononuclear Molybdenum Enzymes. *Chem. Rev.* **2014,** *114* (7), 3963-4038.
88. Liu, M.; Nazemi, A.; Taylor, M. G.; Nandy, A.; Duan, C.; Steeves, A. H.; Kulik, H. J., Large-Scale Screening Reveals That Geometric Structure Matters More Than Electronic Structure in the Bioinspired Catalyst Design of Formate Dehydrogenase Mimics. *ACS Catal.* **2021,** *12* (1), 383-396.
89. Kniemeyer, O.; Heider, J., Ethylbenzene Dehydrogenase, a Novel Hydrocarbon-Oxidizing Molybdenum/Iron-Sulfur/Heme Enzyme. *J. Biol. Chem.* **2001,** *276*, 21381–21386.
90. Hagel, C.; Blaum, B.; Friedrich, T.; Heider1, J., Characterisation of the Redox Centers of Ethylbenzene Dehydrogenase. *J. Biol. Inorg. Chem.* **2022,** *27*, 143–154.
91. Szaleniec, M.; Borowski, T.; Schuhle, K.; Witko, M.; Heider, J., Ab Initio Modeling of Ethylbenzene Dehydrogenase Reaction Mechanism. *J. Am. Chem. Soc.* **2010,** *132*, 6014–6024.
92. Szaleniec, M.; Salwiński, A.; Borowski, T.; Heider, J.; Witko, M., Quantum Chemical Modeling Studies of Ethylbenzene Dehydrogenase Activity. *Int. J. Quantum Chem.* **2012,** *112* (8), 1990-1999.

93. Szaleniec, M.; Dudzik, A.; Kozik, B.; Borowski, T.; Heider, J.; Witko, M., Mechanistic Basis for the Enantioselectivity of the Anaerobic Hydroxylation of Alkylaromatic Compounds by Ethylbenzene Dehydrogenase. *J. Inorg. Biochem.* **2014,** *139*, 9-20.
94. Warnke, M.; Jung, T.; Dermer, J.; Hipp, K.; Jehmlich, N.; Bergen, M. v.; Ferlaino, S.; Fries, A.; Mîller, M.; Boll, M., 25-Hydroxyvitamin D3 Synthesis by Enzymatic Steroid Side-Chain Hydroxylation with Water. *Angew. Chem. Int. Ed.* **2016,** *55*, 1881 –1884.
95. Rugor, A.; Wójcik-Augustyn, A.; Niedzialkowska, E.; Mordalski, S.; Staroń, J.; Bojarski, A.; Szaleniec, M., Reaction Mechanism of Sterol Hydroxylation by Steroid C25 Dehydrogenase – Homology Model, Reactivity and Isoenzymatic Diversity. *J. Inorg. Biochem.* **2017,** *173*, 28-43.
96. Martinie, R. J.; Pollock, C. J.; Matthews, M. L.; Bollinger, J. M.; Krebs, C.; Silakov, A., Vanadyl as a Stable Structural Mimic of Reactive Ferryl Intermediates in Mononuclear Nonheme-Iron Enzymes. *Inorg. Chem.* **2017,** *56* (21), 13382-13389.
97. Agarwal, V.; Miles, Z. D.; Winter, J. M.; Eustáquio, A. S.; El Gamal, A. A.; Moore, B. S., Enzymatic Halogenation and Dehalogenation Reactions: Pervasive and Mechanistically Diverse. *Chem. Rev.* **2017,** *117* (8), 5619-5674.
98. McCracken, J.; Casey, T. M.; Hausinger, R. P., H-1-HYSCORE Reveals Structural Details at the Fe(II) Active Site of Taurine:2-Oxoglutarate Dioxygenase. *Appl. Magn. Reson.* **2021,** *52* (8), 971-994.
99. Bell, C. B.; Wong, S. D.; Xiao, Y.; Klinker, E. J.; Tenderholt, A. L.; Smith, M. C.; Rohde, J.-U.; Que, L., Jr.; Cramer, S. P.; Solomon, E. I., A Combined NRVS and DFT Study of $Fe^{IV}$=O Model Complexes: a Diagnostic Method for the Elucidation of Non-Heme Iron Enzyme Intermediates. *Angew. Chem. Int. Ed.* **2008,** *47* (47), 9071-9074.
100. Gupta, R.; Lacy, D. C.; Bominaar, E. L.; Borovik, A. S.; Hendrich, M. P., EPR and Mössbauer Spectroscopy, and DFT Analysis of a High-Spin $Fe^{IV}$-oxo Complex. *J. Am. Chem. Soc.* **2012,** *134* (23), 9775-9784.
101. Leu, B. M.; Zgierski, M. Z.; Wyllie, G. R. A.; Scheidt, W. R.; Sturhahn, W.; Alp, E. E.; Durbin, S. M.; Sage, J. T., Quantitative Vibrational Dynamics of Iron in Nitrosyl Porphyrins. *J. Am. Chem. Soc.* **2004,** *126* (13), 4211-4227.
102. Srnec, M.; Iyer, S. R.; Dassama, L. M. K.; Park, K.; Wong, S. D.; Sutherlin, K. D.; Yoshitaka, Y.; Kobayashi, Y.; Kurokuzu, M.; Saito, M.; Seto, M.; Krebs, C.; Bollinger, J. M., Jr.; Solomon, E. I., NRVS Definition of the Facial Triad $Fe^{IV}$=O Intermediate in Taurine Dioxygenase: Evaluation of Structural Contributions to Hydrogen Atom Abstraction. *J. Am. Chem. Soc.* **2020,** *142* (44), 18886-18896.
103. Srnec, M.; Wong, S. D.; Matthews, M. L.; Krebs, C.; Bollinger, J. M., Jr.; Solomon, E. I., Electronic Structure of the Ferryl Intermediate in the α-Ketoglutarate Dependent Non-Heme Iron Halogenase SyrB2: Contributions to H Atom Abstraction Reactivity. *J. Am. Chem. Soc.* **2016,** *138* (15), 5110-5122.
104. Winkler, J. R.; Gray, H. B., Electronic Structures of Oxo-Metal Ions. **2011,** *142*, 17-28.
105. Ballhausen, C. J.; Gray, H. B., The Electronic Structure of the Vanadyl Ion. *Inorg. Chem.* **1962,** *1* (1), 111-122.
106. Larson, V. A.; Battistella, B.; Ray, K.; Lehnert, N.; Nam, W., Iron and Manganese Oxo Complexes, Oxo Wall and Beyond. *Nat. Rev. Chem.* **2020,** *4* (8), 404-419.
107. Nandy, A.; Kulik, H. J., Why Conventional Design Rules for C–H Activation Fail for Open-Shell Transition-Metal Catalysts. *ACS Catal.* **2020,** *10* (24), 15033-15047.

108. Andris, E.; Navrátil, R.; Jašík, J.; Srnec, M.; Rodríguez, M.; Costas, M.; Roithová, J., M−O Bonding Beyond the Oxo Wall: Spectroscopy and Reactivity of Cobalt(III)-Oxyl and Cobalt(III)-Oxo Complexes. *Angew. Chem. Int. Ed.* **2019,** *58* (28), 9619-9624.
109. Andris, E.; Navrátil, R.; Jašík, J.; Puri, M.; Costas, M.; Que, L.; Roithová, J., Trapping Iron(III)–Oxo Species at the Boundary of the "Oxo Wall": Insights into the Nature of the Fe(III)–O Bond. *J. Am. Chem. Soc.* **2018,** *140* (43), 14391-14400.
110. Dydio, P.; Key, H. M.; Nazarenko, A.; Rha, J. Y. E.; Seyedkazemi, V.; Clark, D. S.; Hartwig, J. F., An Artificial Metalloenzyme with the Kinetics of Native Enzymes. *Science* **2016,** *354* (6308), 102-106.
111. Jensen, K.; Jensen, P. E.; Møller, B. L., Light-Driven Cytochrome P450 Hydroxylations. *ACS Chem. Biol.* **2011,** *6* (6), 533-539.
112. Hirao, H.; Que, L.; Nam, W.; Shaik, S., A Two-State Reactivity Rationale for Counterintuitive Axial Ligand Effects on the C-H Activation Reactivity of Nonheme $Fe^{IV}O$ Oxidants. *Chem. Eur. J.* **2008,** *14* (6), 1740-1756.
113. Ye, S.; Tuttle, T.; Bill, E.; Simkhovich, L.; Gross, Z.; Thiel, W.; Neese, F., The Electronic Structure of Iron Corroles: A Combined Experimental and Quantum Chemical Study. *Chem. Eur. J.* **2008,** *14* (34), 10839-10851.
114. Cho, K.; Leeladee, P.; McGown, A. J.; DeBeer, S.; Goldberg, D. P., A High-Valent Iron–Oxo Corrolazine Activates C–H Bonds via Hydrogen-Atom Transfer. *J. Am. Chem. Soc.* **2012,** *134* (17), 7392-7399.
115. Cho, J.; Sarangi, R.; Nam, W., Mononuclear Metal–$O_2$ Complexes Bearing Macrocyclic N-Tetramethylated Cyclam Ligands. *Acc. Chem. Res.* **2012,** *45* (8), 1321-1330.
116. Singh, R.; Ganguly, G.; Malinkin, S. O.; Demeshko, S.; Meyer, F.; Nordlander, E.; Paine, T. K., A Mononuclear Nonheme Iron(IV)-Oxo Complex of a Substituted N4Py Ligand: Effect of Ligand Field on Oxygen Atom Transfer and C–H Bond Cleavage Reactivity. *Inorg. Chem.* **2019,** *58* (3), 1862-1876.
117. Kazaryan, A.; Baerends, E. J., Ligand Field Effects and the High Spin–High Reactivity Correlation in the H Abstraction by Non-Heme Iron(IV)–Oxo Complexes: A DFT Frontier Orbital Perspective. *ACS Catal.* **2015,** *5* (3), 1475-1488.
118. Schröder, D.; Shaik, S.; Schwarz, H., Two-State Reactivity as a New Concept in Organometallic Chemistry. *Acc. Chem. Res.* **2000,** *33* (3), 139-145.
119. Janardanan, D.; Usharani, D.; Shaik, S., The Origins of Dramatic Axial Ligand Effects: Closed-Shell $Mn^{V}O$ Complexes Use Exchange-Enhanced Open-Shell States to Mediate Efficient H Abstraction Reactions. *Angew. Chem. Int. Ed.* **2012,** *51* (18), 4421-4425.
120. Puri, M.; Que, L., Toward the Synthesis of More Reactive S = 2 Non-Heme Oxoiron(IV) Complexes. *Acc. Chem. Res.* **2015,** *48* (8), 2443-2452.
121. Seo, M. S.; Kim, N. H.; Cho, K.-B.; So, J. E.; Park, S. K.; Clémancey, M.; Garcia-Serres, R.; Latour, J.-M.; Shaik, S.; Nam, W., A Mononuclear Nonheme Iron(IV)-Oxo Complex Which is More Reactive than Cytochrome P450 Model Compound I. *Chem. Sci.* **2011,** *2* (6), 1039.
122. Kupper, C.; Mondal, B.; Serrano-Plana, J.; Klawitter, I.; Neese, F.; Costas, M.; Ye, S.; Meyer, F., Nonclassical Single-State Reactivity of an Oxo-Iron(IV) Complex Confined to Triplet Pathways. *J. Am. Chem. Soc.* **2017,** *139* (26), 8939-8949.
123. Monte Pérez, I.; Engelmann, X.; Lee, Y.-M.; Yoo, M.; Kumaran, E.; Farquhar, E. R.; Bill, E.; England, J.; Nam, W.; Swart, M.; Ray, K., A Highly Reactive Oxoiron(IV) Complex Supported by a Bioinspired $N_3O$ Macrocyclic Ligand. *Angew. Chem. Int. Ed.* **2017,** *56* (46), 14384-14388.

124. Wang, B.; Lee, Y.-M.; Tcho, W.-Y.; Tussupbayev, S.; Kim, S.-T.; Kim, Y.; Seo, M. S.; Cho, K.-B.; Dede, Y.; Keegan, B. C.; Ogura, T.; Kim, S. H.; Ohta, T.; Baik, M.-H.; Ray, K.; Shearer, J.; Nam, W., Synthesis and Reactivity of a Mononuclear Non-Haem Cobalt(IV)-Oxo Complex. *Nat. Commun.* **2017,** *8*, 14839.
125. Massie, A. A.; Denler, M. C.; Cardoso, L. T.; Walker, A. N.; Hossain, M. K.; Day, V. W.; Nordlander, E.; Jackson, T. A., Equatorial Ligand Perturbations Influence the Reactivity of Manganese(IV)-Oxo Complexes. *Angew. Chem. Int. Ed.* **2017,** *56* (15), 4178-4182.
126. Denler, M. C.; Massie, A. A.; Singh, R.; Stewart-Jones, E.; Sinha, A.; Day, V. W.; Nordlander, E.; Jackson, T. A., $Mn^{IV}$-Oxo Complex of a Bis(benzimidazolyl)-Containing N5 Ligand Reveals Different Reactivity Trends for $Mn^{IV}$-Oxo than $Fe^{IV}$-Oxo Species. *Dalton Trans.* **2019,** *48* (15), 5007-5021.
127. Rice, D. B.; Massie, A. A.; Jackson, T. A., Experimental and Multireference Ab Initio Investigations of Hydrogen-Atom-Transfer Reactivity of a Mononuclear $Mn^{IV}$-Oxo Complex. *Inorg. Chem.* **2019,** *58* (20), 13902-13916.
128. Massie, A. A.; Sinha, A.; Parham, J. D.; Nordlander, E.; Jackson, T. A., Relationship between Hydrogen-Atom Transfer Driving Force and Reaction Rates for an Oxomanganese(IV) Adduct. *Inorg. Chem.* **2018,** *57* (14), 8253-8263.
129. Nandy, A.; Duan, C.; Goffinet, C.; Kulik, H., New Strategies for Direct Methane-to-Methanol Conversion from Active Learning Exploration of 16 Million Catalysts. *JACS Au* **2022,** *2* (5), 1200-1213.
130. Ye, S.; Neese, F., Nonheme Oxo-Iron(IV) Intermediates Form an Oxyl Radical upon Approaching the C–H bond Activation Transition State. *Proc. Natl. Acad. Sci. U.S.A.* **2011,** *108* (4), 1228-1233.
131. Geng, C.; Ye, S.; Neese, F., Analysis of Reaction Channels for Alkane Hydroxylation by Nonheme Iron(IV)-Oxo Complexes. *Angew. Chem. Int. Ed.* **2010,** *49* (33), 5717-5720.
132. Geng, C.; Ye, S.; Neese, F., Does a Higher Metal Oxidation State Necessarily Imply Higher Reactivity Toward H-atom Transfer? A Computational Study of C–H Bond Oxidation by High-Valent Iron-Oxo and -Nitrido Complexes. *Dalton Trans.* **2014,** *43* (16), 6079.
133. Maldonado-Domínguez, M.; Srnec, M., Understanding and Predicting Post H-Atom Abstraction Selectivity through Reactive Mode Composition Factor Analysis. *J. Am. Chem. Soc.* **2020,** *142* (8), 3947-3958.
134. Borovik, A. S., Role of Metal–Oxo Complexes in the Cleavage of C–H Bonds. *Chem. Soc. Rev.* **2011,** *40* (4), 1870.
135. Xue, X.-S.; Ji, P.; Zhou, B.; Cheng, J.-P., The Essential Role of Bond Energetics in C–H Activation/Functionalization. *Chem. Rev.* **2017,** *117* (13), 8622-8648.
136. Warren, J. J.; Tronic, T. A.; Mayer, J. M., Thermochemistry of Proton-Coupled Electron Transfer Reagents and Its Implications. *Chem. Rev.* **2010,** *110*, 6961–7001.
137. Klein, J. E. M. N.; Dereli, B.; Que, L.; Cramer, C. J., Why Metal–Oxos React with Dihydroanthracene and Cyclohexadiene at Comparable Rates, Despite Having Different C–H bond strengths. A Computational Study. *Chem. Commun.* **2016,** *52* (69), 10509-10512.
138. Mayer, J. M., Hydrogen Atom Abstraction by Metal–Oxo Complexes: Understanding the Analogy with Organic Radical Reactions. *Acc. Chem. Res.* **1998,** *31*, 441–450.
139. Mayer, J. M.; Rhile, I. J., Thermodynamics and Kinetics of Proton-Coupled Electron Transfer: Stepwise vs. Concerted Pathways. *Biochim. Biophys. Acta Bioenerg.* **2004,** *1655*, 51-58.

140. Hammes-Schiffer, S.; Stuchebrukhov, A. A., Theory of Coupled Electron and Proton Transfer Reactions. *Chem. Rev.* **2010,** *110* (12), 6939-6960.
141. Darcy, J. W.; Kolmar, S. S.; Mayer, J. M., Transition State Asymmetry in C–H Bond Cleavage by Proton-Coupled Electron Transfer. *J. Am. Chem. Soc.* **2019,** *141* (27), 10777-10787.
142. Goetz, M. K.; Anderson, J. S., Experimental Evidence for $pK_a$-Driven Asynchronicity in C–H Activation by a Terminal Co(III)–Oxo Complex. *J. Am. Chem. Soc.* **2019,** *141* (9), 4051-4062.
143. Kang, Y.; Chen, H.; Jeong, Y. J.; Lai, W.; Bae, E. H.; Shaik, S.; Nam, W., Enhanced Reactivities of Iron(IV)-Oxo Porphyrin π-Cation Radicals in Oxygenation Reactions by Electron-Donating Axial Ligands. *Chem. Eur. J.* **2009,** *15* (39), 10039-10046.
144. Tang, H.; Guan, J.; Liu, H.; Huang, X., Comparative Insight into Electronic Properties and Reactivities toward C–H Bond Activation by Iron(IV)–Nitrido, Iron(IV)–Oxo, and Iron(IV)–Sulfido Complexes: A Theoretical Investigation. *Inorg. Chem.* **2013,** *52* (5), 2684-2696.
145. Visser, S. P. d., Trends in Substrate Hydroxylation Reactions by Heme and Nonheme Iron(IV)-oxo Oxidants Give Correlations Between Intrinsic Properties of the Oxidant with Barrier Height. *J. Am. Chem. Soc.* **2010,** *132*, 1087–1097.
146. Bryant, J. R.; Mayer, J. M., Oxidation of C-H bonds by $[(bpy)_2(py)Ru^{IV}O]^{2+}$ Occurs by Hydrogen Atom Abstraction. *J. Am. Chem. Soc.* **2003,** *125*, 10351-10361.
147. Kotani, H.; Kaida, S.; Ishizuka, T.; Mieda, K.; Sakaguchi, M.; Ogura, T.; Shiota, Y.; Yoshizawa, K.; Kojima, T., Importance of the Reactant-State Potentials of Chromium(V)–Oxo Complexes to Determine the Reactivity in Hydrogen-Atom Transfer Reactions. *Inorg. Chem.* **2018,** *57* (21), 13929-13936.
148. Bell, R. P., The Theory of Reactions Involving Proton Transfers. *Proc. R. Soc. London, Ser. A* **1936,** *154* (882), 414-429.
149. Evans, M. G.; Polanyi, M., Inertia and Driving Force of Chemical Reactions *Trans. Faraday Soc.* **1938,** *34*, 11-24.
150. Bím, D.; Maldonado-Domínguez, M.; Rulíšek, L.; Srnec, M., Beyond the Classical Thermodynamic Contributions to Hydrogen Atom Abstraction Reactivity. *Proc. Natl. Acad. Sci. U.S.A.* **2018,** *115*, 10287-10294.
151. Nazemi, A.; Cundari, T. R., Control of C–H Bond Activation by Mo-Oxo Complexes: $pK_a$ or Bond Dissociation Free Energy (BDFE)? *Inorg. Chem.* **2017,** *56* (20), 12319-12327.
152. Kotani, H.; Shimomura, H.; Ikeda, K.; Ishizuka, T.; Shiota, Y.; Yoshizawa, K.; Kojima, T., Mechanistic Insight into Concerted Proton–Electron Transfer of a Ru(IV)-Oxo Complex: A Possible Oxidative Asynchronicity. *J. Am. Chem. Soc.* **2020,** *142* (40), 16982-16989.
153. Mandal, M.; Elwell, C. E.; Bouchey, C. J.; Zerk, T. J.; Tolman, W. B.; Cramer, C. J., Mechanisms for Hydrogen-Atom Abstraction by Mononuclear Copper(III) Cores: Hydrogen-Atom Transfer or Concerted Proton-Coupled Electron Transfer? *J. Am. Chem. Soc.* **2019,** *141* (43), 17236-17244.
154. Barman, S. K.; Yang, M.-Y.; Parsell, T. H.; Green, M. T.; Borovik, A. S., Semiempirical Method for Examining Asynchronicity in Metal–Oxido-Mediated C–H Bond Activation. *Proc. Natl. Acad. Sci. U.S.A.* **2021,** *118* (36), e2108648118.
155. Dietl, N.; Schlangen, M.; Schwarz, H., Thermal Hydrogen-Atom Transfer from Methane: The Role of Radicals and Spin States in Oxo-Cluster Chemistry. *Angew. Chem. Int. Ed.* **2012,** *51* (23), 5544-5555.
156. Saouma, C. T.; Mayer, J. M., Do Spin State and Spin Density Affect Hydrogen Atom Transfer Reactivity? *Chem. Sci.* **2014,** *5* (1), 21-31.

157. Gani, T. Z. H.; Kulik, H. J., Understanding and Breaking Scaling Relations in Single-Site Catalysis: Methane to Methanol Conversion by $Fe^{IV}$=O. *ACS Catal.* **2018,** *8* (2), 975-986.
158. Nandy, A.; Zhu, J.; Janet, J. P.; Duan, C.; Getman, R. B.; Kulik, H. J., Machine Learning Accelerates the Discovery of Design Rules and Exceptions in Stable Metal–Oxo Intermediate Formation. *ACS Catal.* **2019,** *9* (9), 8243-8255.
159. Schneider, J. E.; Goetz, M. K.; Anderson, J. S., Statistical Analysis of C–H Activation by Oxo Complexes Supports Diverse Thermodynamic Control Over Reactivity. *Chem. Sci.* **2021,** *12* (11), 4173-4183.
160. Klinman, J. P.; Offenbacher, A. R., Understanding Biological Hydrogen Transfer Through the Lens of Temperature Dependent Kinetic Isotope Effects. *Acc. Chem. Res.* **2018,** *51* (9), 1966-1974.
161. Dutra, M.; Amaya, J. A.; McElhenney, S.; Manley, O. M.; Makris, T. M.; Rassolov, V.; Garashchuk, S., Experimental and Theoretical Examination of the Kinetic Isotope Effect in Cytochrome P450 Decarboxylase OleT. *J. Phys. Chem. B* **2022,** *126* (19), 3493-3504.
162. Klein, J. E. M. N.; Mandal, D.; Ching, W.-M.; Mallick, D.; Que, L.; Shaik, S., Privileged Role of Thiolate as the Axial Ligand in Hydrogen Atom Transfer Reactions by Oxoiron(IV) Complexes in Shaping the Potential Energy Surface and Inducing Significant H-Atom Tunneling. *J. Am. Chem. Soc.* **2017,** *139* (51), 18705-18713.
163. Li, J.; Corma, A.; Yu, J., Synthesis of New Zeolite Structures. *Chem. Soc. Rev.* **2015,** *44* (20), 7112-7127.
164. Li, G.; Pidko, E. A.; van Santen, R. A.; Li, C.; Hensen, E. J. M., Stability of Extraframework Iron-Containing Complexes in ZSM-5 Zeolite. *J. Phys. Chem. C* **2012,** *117* (1), 413-426.
165. Bols, M. L.; Hallaert, S. D.; Snyder, B. E. R.; Devos, J.; Plessers, D.; Rhoda, H. M.; Dusselier, M.; Schoonheydt, R. A.; Pierloot, K.; Solomon, E. I.; Sels, B. F., Spectroscopic Identification of the α-Fe/α-O Active Site in Fe-CHA Zeolite for the Low-Temperature Activation of the Methane C–H Bond. *J. Am. Chem. Soc.* **2018,** *140* (38), 12021-12032.
166. Szécsényi, Á.; Li, G.; Gascon, J.; Pidko, E. A., Mechanistic Complexity of Methane Oxidation with $H_2O_2$ by Single-Site Fe/ZSM-5 Catalyst. *ACS Catal.* **2018,** *8* (9), 7961-7972.
167. Pannov, G. I.; Sobolev, V. I.; Kharitonov, A. S., The Role of Iron in $N_2O$ Decomposition on ZSM-5 Zeolite and Reactivity of the Surface Oxygen Formed. *J. Mol. Catal.* **1990,** *61* (1), 85-97.
168. Snyder, B. E. R.; Vanelderen, P.; Bols, M. L.; Hallaert, S. D.; Böttger, L. H.; Ungur, L.; Pierloot, K.; Schoonheydt, R. A.; Sels, B. F.; Solomon, E. I., The Active Site of Low-Temperature Methane Hydroxylation in Iron-Containing Zeolites. *Nature* **2016,** *536* (7616), 317-321.
169. Snyder, B. E. R.; Böttger, L. H.; Bols, M. L.; Yan, J. J.; Rhoda, H. M.; Jacobs, A. B.; Hu, M. Y.; Zhao, J.; Alp, E. E.; Hedman, B.; Hodgson, K. O.; Schoonheydt, R. A.; Sels, B. F.; Solomon, E. I., Structural Characterization of a Non-Heme Iron Active Site in Zeolites that Hydroxylates Methane. *Proc. Natl. Acad. Sci. U.S.A.* **2018,** *115* (18), 4565-4570.
170. Hammond, C.; Forde, M. M.; Ab Rahim, M. H.; Thetford, A.; He, Q.; Jenkins, R. L.; Dimitratos, N.; Lopez-Sanchez, J. A.; Dummer, N. F.; Murphy, D. M.; Carley, A. F.; Taylor, S. H.; Willock, D. J.; Stangland, E. E.; Kang, J.; Hagen, H.; Kiely, C. J.; Hutchings, G. J., Direct Catalytic Conversion of Methane to Methanol in an Aqueous Medium by using Copper-Promoted Fe-ZSM-5. *Angew. Chem. Int. Ed.* **2012,** *51* (21), 5129-5133.

171. Groothaert, M. H.; Smeets, P. J.; Sels, B. F.; Jacobs, P. A.; Schoonheydt, R. A., Selective Oxidation of Methane by the Bis (μ-oxo) Dicopper Core Stabilized on ZSM-5 and Mordenite Zeolites. *J. Am. Chem. Soc.* **2005,** *127* (5), 1394-1395.
172. Narsimhan, K.; Iyoki, K.; Dinh, K.; Román-Leshkov, Y., Catalytic Oxidation of Methane into Methanol over Copper-Exchanged Zeolites with Oxygen at Low Temperature. *ACS Cent. Sci.* **2016,** *2* (6), 424-429.
173. Tabor, E.; Dedecek, J.; Mlekodaj, K.; Sobalik, Z.; Andrikopoulos, P. C.; Sklenak, S., Dioxygen Dissociation Over Man-Made System at Room Temperature to Form the Active α-Oxygen for Methane Oxidation. *Sci. Adv.* **2020,** *6* (20), eaaz9776.
174. Tabor, E.; Lemishka, M.; Olszowka, J. E.; Mlekodaj, K.; Dedecek, J.; Andrikopoulos, P. C.; Sklenak, S., Splitting Dioxygen over Distant Binuclear Fe Sites in Zeolites. Effect of the Local Arrangement and Framework Topology. *ACS Catal.* **2021,** *11* (4), 2340-2355.
175. Grundner, S.; Markovits, M. A. C.; Li, G.; Tromp, M.; Pidko, E. A.; Hensen, E. J. M.; Jentys, A.; Sanchez-Sanchez, M.; Lercher, J. A., Single-Site Trinuclear Copper Oxygen Clusters in Mordenite for Selective Conversion of Methane to Methanol. *Nat. Commun.* **2015,** *6* (1), 7546.
176. Vanelderen, P.; Snyder, B. E. R.; Tsai, M.-L.; Hadt, R. G.; Vancauwenbergh, J.; Coussens, O.; Schoonheydt, R. A.; Sels, B. F.; Solomon, E. I., Spectroscopic Definition of the Copper Active Sites in Mordenite: Selective Methane Oxidation. *J. Am. Chem. Soc.* **2015,** *137* (19), 6383-6392.
177. Mahyuddin, M. H.; Tanaka, T.; Shiota, Y.; Staykov, A.; Yoshizawa, K., Methane Partial Oxidation Over $[Cu_2(\mu\text{-}O)]^{2+}$ and $[Cu_3(\mu\text{-}O)_3]^{2+}$ Active Species in Large-Pore Zeolites. *ACS Catal.* **2018,** *8* (2), 1500-1509.
178. Vennelakanti, V.; Nandy, A.; Kulik, H. J., The Effect of Hartree-Fock Exchange on Scaling Relations and Reaction Energetics for C-H Activation Catalysts. *Top. Catal.* **2022,** *65* (1-4), 296-311.
179. Zhou, H.-C.; Long, J. R.; Yaghi, O. M., Introduction to Metal–Organic Frameworks. *Chem. Rev.* **2012,** *112* (2), 673-674.
180. Bour, J. R.; Wright, A. M.; He, X.; Dincă, M., Bioinspired Chemistry at MOF Secondary Building Units. *Chem. Sci.* **2020,** *11* (7), 1728-1737.
181. Xiao, D. J.; Bloch, E. D.; Mason, J. A.; Queen, W. L.; Hudson, M. R.; Planas, N.; Borycz, J.; Dzubak, A. L.; Verma, P.; Lee, K.; Bonino, F.; Crocellà, V.; Yano, J.; Bordiga, S.; Truhlar, D. G.; Gagliardi, L.; Brown, C. M.; Long, J. R., Oxidation of Ethane to Ethanol by $N_2O$ in a Metal–Organic Framework with Coordinatively Unsaturated Iron(II) Sites. *Nat. Chem.* **2014,** *6* (7), 590-595.
182. Osadchii, D. Y.; Olivos-Suarez, A. I.; Szécsényi, Á.; Li, G.; Nasalevich, M. A.; Dugulan, I. A.; Crespo, P. S.; Hensen, E. J. M.; Veber, S. L.; Fedin, M. V.; Sankar, G.; Pidko, E. A.; Gascon, J., Isolated Fe Sites in Metal Organic Frameworks Catalyze the Direct Conversion of Methane to Methanol. *ACS Catal.* **2018,** *8* (6), 5542-5548.
183. Moghadam, P. Z.; Li, A.; Wiggin, S. B.; Tao, A.; Maloney, A. G. P.; Wood, P. A.; Ward, S. C.; Fairen-Jimenez, D., Development of a Cambridge Structural Database Subset: A Collection of Metal–Organic Frameworks for Past, Present, and Future. *Chem. Mater.* **2017,** *29* (7), 2618-2625.
184. Moosavi, S. M.; Nandy, A.; Jablonka, K. M.; Ongari, D.; Janet, J. P.; Boyd, P. G.; Lee, Y.; Smit, B.; Kulik, H. J., Understanding the Diversity of the Metal-Organic Framework Ecosystem. *Nat. Commun.* **2020,** *11* (1), 4068.

185. Ranocchiari, M.; Lothschütz, C.; Grolimund, D.; van Bokhoven, J. A., Single-Atom Active Sites on Metal-Organic Frameworks. *Proc. R. Soc. London, Ser. A* **2012,** *468* (2143), 1985-1999.
186. Bernales, V.; Ortuño, M. A.; Truhlar, D. G.; Cramer, C. J.; Gagliardi, L., Computational Design of Functionalized Metal–Organic Framework Nodes for Catalysis. *ACS Cent. Sci.* **2018,** *4* (1), 5-19.
187. Verma, P.; Vogiatzis, K. D.; Planas, N.; Borycz, J.; Xiao, D. J.; Long, J. R.; Gagliardi, L.; Truhlar, D. G., Mechanism of Oxidation of Ethane to Ethanol at Iron(IV)–Oxo Sites in Magnesium-Diluted $Fe_2$(dobdc). *J. Am. Chem. Soc.* **2015,** *137* (17), 5770-5781.
188. Rosen, A. S.; Notestein, J. M.; Snurr, R. Q., Identifying Promising Metal–Organic Frameworks for Heterogeneous Catalysis via High-Throughput Periodic Density Functional Theory. *J. Comput. Chem.* **2019,** *40* (12), 1305-1318.
189. Hirao, H.; Ng, W. K. H.; Moeljadi, A. M. P.; Bureekaew, S., Multiscale Model for a Metal–Organic Framework: High-Spin Rebound Mechanism in the Reaction of the Oxoiron(IV) Species of Fe-MOF-74. *ACS Catal.* **2015,** *5* (6), 3287-3291.
190. Moeljadi, A. M. P.; Schmid, R.; Hirao, H., Dioxygen Binding to Fe-MOF-74: Microscopic Insights from Periodic QM/MM Calculations. *Can. J. Chem.* **2016,** *94* (12), 1144-1150.
191. Simons, M. C.; Vitillo, J. G.; Babucci, M.; Hoffman, A. S.; Boubnov, A.; Beauvais, M. L.; Chen, Z.; Cramer, C. J.; Chapman, K. W.; Bare, S. R.; Gates, B. C.; Lu, C. C.; Gagliardi, L.; Bhan, A., Structure, Dynamics, and Reactivity for Light Alkane Oxidation of Fe(II) Sites Situated in the Nodes of a Metal–Organic Framework. *J. Am. Chem. Soc.* **2019,** *141* (45), 18142-18151.
192. Simons, M. C.; Prinslow, S. D.; Babucci, M.; Hoffman, A. S.; Hong, J.; Vitillo, J. G.; Bare, S. R.; Gates, B. C.; Lu, C. C.; Gagliardi, L.; Bhan, A., Beyond Radical Rebound: Methane Oxidation to Methanol Catalyzed by Iron Species in Metal–Organic Framework Nodes. *J. Am. Chem. Soc.* **2021,** *143* (31), 12165-12174.
193. Shabbir, H.; Vicchio, S. P.; Meza-Morales, P.; Getman, R. B., Role of Molecular Simulations in the Design of Metal–Organic Frameworks for Gas-Phase Thermocatalysis: A Perspective. *J. Phys. Chem. C* **2022,** *126* (13), 6111-6118.
194. Zhang, X.; Huang, Z.; Ferrandon, M.; Yang, D.; Robison, L.; Li, P.; Wang, T. C.; Delferro, M.; Farha, O. K., Catalytic Chemoselective Functionalization of Methane in a Metal–Organic Framework. *Nat. Catal.* **2018,** *1* (5), 356-362.
195. Cook, A. K.; Schimler, S. D.; Matzger, A. J.; Sanford, M. S., Catalyst-Controlled Selectivity in the C-H Borylation of Methane and Ethane. *Science* **2016,** *351* (6280), 1421-1424.
196. Dissegna, S.; Epp, K.; Heinz, W. R.; Kieslich, G.; Fischer, R. A., Defective Metal-Organic Frameworks. *Adv. Mater.* **2018,** *30* (37), 1704501.
197. Yang, D.; Babucci, M.; Casey, W. H.; Gates, B. C., The Surface Chemistry of Metal Oxide Clusters: From Metal–Organic Frameworks to Minerals. *ACS Cent. Sci.* **2020,** *6* (9), 1523-1533.
198. Liu, Y.; Klet, R. C.; Hupp, J. T.; Farha, O., Probing the Correlations Between the Defects in Metal–Organic Frameworks and their Catalytic Activity by an Epoxide Ring-Opening Reaction. *Chem. Commun.* **2016,** *52* (50), 7806-7809.
199. Park, T.-H.; Hickman, A. J.; Koh, K.; Martin, S.; Wong-Foy, A. G.; Sanford, M. S.; Matzger, A. J., Highly Dispersed Palladium(II) in a Defective Metal–Organic Framework:

Application to C–H Activation and Functionalization. *J. Am. Chem. Soc.* **2011,** *133* (50), 20138-20141.
200. Nandy, A.; Duan, C.; Kulik, H. J., Using Machine Learning and Data Mining to Leverage Community Knowledge for the Engineering of Stable Metal–Organic Frameworks. *J. Am. Chem. Soc.* **2021,** *143* (42), 17535-17547.
201. Wu, G.; Johnston, C. M.; Mack, N. H.; Artyushkova, K.; Ferrandon, M.; Nelson, M.; Lezama-Pacheco, J. S.; Conradson, S. D.; More, K. L.; Myers, D. J.; Zelenay, P., Synthesis-Structure-Performance Correlation for Polyaniline-Me-C Non-Precious Metal Cathode Catalysts for Oxygen Reduction in Fuel Cells. *J. Mater. Chem.* **2011,** *21* (30), 11392-11405.
202. Fei, H. L.; Dong, J. C.; Arellano-Jimenez, M. J.; Ye, G. L.; Kim, N. D.; Samuel, E. L. G.; Peng, Z. W.; Zhu, Z.; Qin, F.; Bao, J. M.; Yacaman, M. J.; Ajayan, P. M.; Chen, D. L.; Tour, J. M., Atomic Cobalt on Nitrogen-Doped Graphene for Hydrogen Generation. *Nat. Commun.* **2015,** *6*, 8668.
203. Kramm, U. I.; Abs-Wurmbach, I.; Herrmann-Geppert, I.; Radnik, J.; Fiechter, S.; Bogdanoff, P., Influence of the Electron-Density of FeN4-Centers Towards the Catalytic Activity of Pyrolyzed FeTMPPCl-Based ORR-Electrocatalysts. *J. Electrochem. Soc.* **2011,** *158* (1), B69-B78.
204. Deng, D. H.; Chen, X. Q.; Yu, L.; Wu, X.; Liu, Q. F.; Liu, Y.; Yang, H. X.; Tian, H. F.; Hu, Y. F.; Du, P. P.; Si, R.; Wang, J. H.; Cui, X. J.; Li, H. B.; Xiao, J. P.; Xu, T.; Deng, J.; Yang, F.; Duchesne, P. N.; Zhang, P.; Zhou, J. G.; Sun, L. T.; Li, J. Q.; Pan, X. L.; Bao, X. H., A Single Iron Site Confined in a Graphene Matrix for the Catalytic Oxidation of Benzene at Room Temperature. *Sci. Adv.* **2015,** *1* (11), e1500462.
205. Zhang, C. H.; Yang, S. Z.; Wu, J. J.; Liu, M. J.; Yazdi, S.; Ren, M. Q.; Sha, J. W.; Zhong, J.; Nie, K. Q.; Jalilov, A. S.; Li, Z. Y.; Li, H. M.; Yakobson, B. I.; Wu, Q.; Ringe, E. L.; Xu, H.; Ajayan, P. M.; Tour, J. M., Electrochemical $CO_2$ Reduction with Atomic Iron-Dispersed on Nitrogen-Doped Graphene. *Adv. Energy Mater.* **2018,** *8* (19), 1703487.
206. Dzara, M. J.; Artyushkova, K.; Sougrati, M. T.; Ngo, C.; Fitzgerald, M. A.; Serov, A.; Zulevi, B.; Atanassov, P.; Jaouen, F.; Pylypenko, S., Characterizing Complex Gas-Solid Interfaces with in Situ Spectroscopy: Oxygen Adsorption Behavior on Fe-N-C Catalysts. *J. Phys. Chem. C* **2020,** *124* (30), 16529-16543.
207. Liu, W. G.; Zhang, L. L.; Liu, X.; Liu, X. Y.; Yang, X. F.; Miao, S.; Wang, W. T.; Wang, A. Q.; Zhang, T., Discriminating Catalytically Active FeNx Species of Atomically Dispersed Fe-N-C Catalyst for Selective Oxidation of the C-H Bond. *J. Am. Chem. Soc.* **2017,** *139* (31), 10790-10798.
208. Marshall-Roth, T.; Libretto, N. J.; Wrobel, A. T.; Anderton, K. J.; Pegis, M. L.; Ricke, N. D.; Voorhis, T. V.; Miller, J. T.; Surendranath, Y., A Pyridinic Fe-N4 Macrocycle Models the Active Sites in Fe/N-doped Carbon Electrocatalysts. *Nat. Commun.* **2020,** *11* (1), 1-14.
209. Adli, N. M.; Shan, W. T.; Hwang, S.; Samarakoon, W.; Karakalos, S.; Li, Y.; Cullen, D. A.; Su, D.; Feng, Z. X.; Wang, G. F.; Wu, G., Engineering Atomically Dispersed FeN4 Active Sites for CO2 Electroreduction. *Angew. Chem. Int. Ed.* **2021,** *60* (2), 1022-1032.
210. Wang, L.; Liu, X. K.; Cao, L. L.; Zhang, W.; Chen, T.; Lin, Y.; Wang, H. J.; Wang, Y.; Yao, T., Active Sites of Single-Atom Iron Catalyst for Electrochemical Hydrogen Evolution. *J. Phys. Chem. Lett.* **2020,** *11* (16), 6691-6696.
211. Yu, L.; Li, Y. C.; Ruan, Y. F., Dynamic Control of Sacrificial Bond Transformation in the Fe-N-C Single-Atom Catalyst for Molecular Oxygen Reduction. *Angew. Chem. Int. Ed.* **2021,** *60* (48), 25296-25301.

212. Yuan, K.; Lutzenkirchen-Hecht, D.; Li, L. B.; Shuai, L.; Li, Y. Z.; Cao, R.; Qiu, M.; Zhuang, X. D.; Leung, M. K. H.; Chen, Y. W.; Scherf, U., Boosting Oxygen Reduction of Single Iron Active Sites via Geometric and Electronic Engineering: Nitrogen and Phosphorus Dual Coordination. *J. Am. Chem. Soc.* **2020,** *142* (5), 2404-2412.
213. Zitolo, A.; Goellner, V.; Armel, V.; Sougrati, M. T.; Mineva, T.; Stievano, L.; Fonda, E.; Jaouen, F., Identification of Catalytic Sites for Oxygen Reduction in Iron- and Nitrogen-Doped Graphene Materials. *Nat. Mater.* **2015,** *14* (9), 937-942.
214. Patniboon, T.; Hansen, H. A., Acid-Stable and Active M-N-C Catalysts for the Oxygen Reduction Reaction: The Role of Local Structure. *ACS Catal.* **2021,** *11* (21), 13102-13118.
215. Tan, X.; Tahini, H. A.; Smith, S. C., Defect Engineering in Graphene-Confined Single-Atom Iron Catalysts for Room-Temperature Methane Conversion. *J. Phys. Chem. C* **2021,** *125* (23), 12628-12635.
216. Li, J.; Pršlja, P.; Shinagawa, T.; Martín Fernández, A. J.; Krumeich, F.; Artyushkova, K.; Atanassov, P.; Zitolo, A.; Zhou, Y.; García-Muelas, R.; López, N.; Pérez-Ramírez, J.; Jaouen, F., Volcano Trend in Electrocatalytic $CO_2$ Reduction Activity over Atomically Dispersed Metal Sites on Nitrogen-Doped Carbon. *ACS Catal.* **2019,** *9* (11), 10426-10439.
217. Li, X. H.; Yang, X. X.; Liu, L. T.; Zhao, H.; Li, Y. W.; Zhu, H. Y.; Chen, Y. Z.; Guo, S. W.; Liu, Y. N.; Tan, Q.; Wu, G., Chemical Vapor Deposition for N/S-Doped Single Fe Site Catalysts for the Oxygen Reduction in Direct Methanol Fuel Cells. *ACS Catal.* **2021,** *11* (12), 7450-7459.
218. Yang, L.; Cheng, D. J.; Xu, H. X.; Zeng, X. F.; Wan, X.; Shui, J. L.; Xiang, Z. H.; Cao, D. P., Unveiling the High-Activity Origin of Single-Atom Iron Catalysts for Oxygen Reduction Reaction. *Proc. Natl. Acad. Sci. U.S.A.* **2018,** *115* (26), 6626-6631.
219. Zhang, J. Q.; Zhao, Y. F.; Chen, C.; Huang, Y. C.; Dong, C. L.; Chen, C. J.; Liu, R. S.; Wang, C. Y.; Yan, K.; Li, Y. D.; Wang, G. X., Tuning the Coordination Environment in Single-Atom Catalysts to Achieve Highly Efficient Oxygen Reduction Reactions. *J. Am. Chem. Soc.* **2019,** *141* (51), 20118-20126.
220. Pan, F. P.; Li, B. Y.; Sarnello, E.; Fei, Y. H.; Feng, X. H.; Gang, Y.; Xiang, X. M.; Fang, L. Z.; Li, T.; Hu, Y. H.; Wang, G. F.; Li, Y., Pore-Edge Tailoring of Single-Atom Iron-Nitrogen Sites on Graphene for Enhanced $CO_2$ Reduction. *ACS Catal.* **2020,** *10* (19), 10803-10811.
221. Pan, F. P.; Zhang, H. G.; Liu, K. X.; Cullen, D.; More, K.; Wang, M. Y.; Feng, Z. X.; Wang, G. F.; Wu, G.; Li, Y., Unveiling Active Sites of $CO_2$ Reduction on Nitrogen-Coordinated and Atomically Dispersed Iron and Cobalt Catalysts. *ACS Catal.* **2018,** *8* (4), 3116-3122.
222. Cui, X. J.; Li, H. B.; Wang, Y.; Hu, Y. L.; Hua, L.; Li, H. Y.; Han, X. W.; Liu, Q. F.; Yang, F.; He, L. M.; Chen, X. Q.; Li, Q. Y.; Xiao, J. P.; Deng, D. H.; Bao, X. H., Room-Temperature Methane Conversion by Graphene-Confined Single Iron Atoms. *Chem* **2018,** *4* (8), 1902-1910.
223. Woo, J.; Choi, H.; Sa, Y. J.; Kim, H. Y.; Lim, T.; Jang, J. H.; Yoo, S. J.; Kim, J. Y.; Kim, C. S.; Joo, S. H., Structural Evolution of Atomically Dispersed Fe Species in Fe-N/C Catalysts Probed by X-ray Absorption and Fe-57 Mossbauer Spectroscopies. *J. Phys. Chem. C* **2021,** *125* (22), 11928-11938.
224. Li, X. N.; Cao, C. S.; Hung, S. F.; Lu, Y. R.; Cai, W. Z.; Rykov, A. I.; Miao, S.; Xi, S. B.; Yang, H. B.; Hu, Z. H.; Wang, J. H.; Zhao, J. Y.; Alp, E. E.; Xu, W.; Chan, T. S.; Chen, H. M.; Xiong, Q. H.; Xiao, H.; Huang, Y. Q.; Li, J.; Zhang, T.; Liu, B., Identification of the Electronic and Structural Dynamics of Catalytic Centers in Single-Fe-Atom Material. *Chem* **2020,** *6* (12), 3440-3454.

225. Paul, S.; Kao, Y. L.; Ni, L. M.; Ehnert, R.; Herrmann-Geppert, I.; van de Krol, R.; Stark, R. W.; Jaegermann, W.; Kramm, U. I.; Bogdanoff, P., Influence of the Metal Center in M-N-C Catalysts on the $CO_2$ Reduction Reaction on Gas Diffusion Electrodes. *ACS Catal.* **2021,** *11* (9), 5850-5864.
226. Gu, J.; Hsu, C. S.; Bai, L. C.; Chen, H. M.; Hu, X. L., Atomically Dispersed $Fe^{3+}$ sites Catalyze Efficient $CO_2$ Electroreduction to CO. *Science* **2019,** *364* (6445), 1091-+.
227. Mineva, T.; Matanovic, I.; Atanassov, P.; Sougrati, M. T.; Stievano, L.; Clemancey, M.; Kochem, A.; Latour, J. M.; Jaouen, F., Understanding Active Sites in Pyrolyzed Fe-N-C Catalysts for Fuel Cell Cathodes by Bridging Density Functional Theory Calculations and Fe-57 Mossbauer Spectroscopy. *ACS Catal.* **2019,** *9* (10), 9359-9371.
228. Moriya, M.; Takahama, R.; Kamoi, K.; Ohyama, J.; Kawashima, S.; Kojima, R.; Okada, M.; Hayakawa, T.; Nabae, Y., Fourteen-Membered Macrocyclic Fe Complexes Inspired by FeN4-Center-Embedded Graphene for Oxygen Reduction Catalysis. *J. Phys. Chem. C* **2020,** *124* (38), 20730-20735.
229. Ohyama, J.; Moriya, M.; Takahama, R.; Kamoi, K.; Kawashima, S.; Kojima, R.; Hayakawa, T.; Nabae, Y., High Durability of a 14-Membered Hexaaza Macrocyclic Fe Complex for an Acidic Oxygen Reduction Reaction Revealed by In Situ XAS Analysis. *JACS Au* **2021,** *1* (10), 1798-1804.
230. Xi, Y. J.; Heyden, A., Direct Oxidation of Methane to Methanol Enabled by Electronic Atomic Monolayer-Metal Support Interaction. *ACS Catal.* **2019,** *9* (7), 6073-6079.
231. Hong, S.; Mpourmpakis, G., Mechanistic Understanding of Methane-to-Methanol Conversion on Graphene-Stabilized Single-Atom Iron Centers. *Catal. Sci. Technol.* **2021,** *11* (19), 6390-6400.
232. Xu, H. X.; Cheng, D. J.; Cao, D. P.; Zeng, X. C., A Universal Principle for a Rational Design of Single-Atom Electrocatalysts *Nat. Catal.* **2018,** *1* (8), 632-632.
233. Fung, V.; Hu, G. X.; Wu, Z. L.; Jiang, D. E., Descriptors for Hydrogen Evolution on Single Atom Catalysts in Nitrogen-Doped Graphene. *J. Phys. Chem. C* **2020,** *124* (36), 19571-19578.
234. Wu, Q.; Wang, G. J.; Liu, M. J., On the Sensitivity to Density-Functional Approximations for CO Binding Energies of Single-Atom Catalysts in Nitrogen-Doped Graphene. *ChemPhysChem* **2022,** *23* (5), e202100787.
235. Liu, F.; Yang, T. H.; Yang, J.; Xu, E.; Bajaj, A.; Kulik, H. J., Bridging the Homogeneous-Heterogeneous Divide: Modeling Spin for Reactivity in Single Atom Catalysis. *Front. Chem.* **2019,** *7*, 219.
236. Latimer, A. A.; Kulkarni, A. R.; Aljama, H.; Montoya, J. H.; Yoo, J. S.; Tsai, C.; Abild-Pedersen, F.; Studt, F.; Nørskov, J. K., Understanding Trends in C–H Bond Activation in Heterogeneous Catalysis. *Nat. Mater.* **2017,** *16* (2), 225-229.
237. Latimer, A. A.; Aljama, H.; Kakekhani, A.; Yoo, J. S.; Kulkarni, A.; Tsai, C.; Garcia-Melchor, M.; Abild-Pedersen, F.; Nørskov, J. K., Mechanistic Insights into Heterogeneous Methane Activation. *Phys. Chem. Chem. Phys.* **2017,** *19* (5), 3575-3581.
238. Latimer, A. A.; Kakekhani, A.; Kulkarni, A. R.; Nørskov, J. K., Direct Methane to Methanol: The Selectivity–Conversion Limit and Design Strategies. *ACS Catal.* **2018,** *8* (8), 6894-6907.
239. Mayer, J. M., Understanding Hydrogen Atom Transfer: From Bond Strengths to Marcus Theory. *Acc. Chem. Res.* **2011,** *44* (1), 36-46.

240. Liao, P.; Getman, R. B.; Snurr, R. Q., Optimizing Open Iron Sites in Metal–Organic Frameworks for Ethane Oxidation: A First-Principles Study. *ACS Appl. Mater. Interfaces* **2017,** *9* (39), 33484-33492.
241. Barona, M.; Ahn, S.; Morris, W.; Hoover, W.; Notestein, J. M.; Farha, O. K.; Snurr, R. Q., Computational Predictions and Experimental Validation of Alkane Oxidative Dehydrogenation by $Fe_2M$ MOF Nodes. *ACS Catal.* **2020,** *10* (2), 1460-1469.
242. Barona, M.; Snurr, R. Q., Exploring the Tunability of Trimetallic MOF Nodes for Partial Oxidation of Methane to Methanol. *ACS Appl. Mater. Interfaces* **2020,** *12* (25), 28217-28231.
243. Khorshidi, A.; Violet, J.; Hashemi, J.; Peterson, A. A., How Strain Can Break the Scaling Relations of Catalysis. *Nat. Catal.* **2018,** *1* (4), 263-268.
244. Lan, Z.; Mallikarjun Sharada, S., Linear Free Energy Relationships for Transition Metal Chemistry: Case Study of CH Activation with Copper–Oxygen Complexes. *Phys. Chem. Chem. Phys.* **2020,** *22* (14), 7155-7159.
245. Andrikopoulos, P. C.; Michel, C.; Chouzier, S.; Sautet, P., In Silico Screening of Iron-Oxo Catalysts for CH Bond Cleavage. *ACS Catal.* **2015,** *5* (4), 2490-2499.
246. Lan, Z.; Mallikarjun Sharada, S., A Framework for Constructing Linear Free Energy Relationships to Design Molecular Transition Metal Catalysts. *Phys. Chem. Chem. Phys.* **2021,** *23* (29), 15543-15556.
247. Szécsényi, Á.; Khramenkova, E.; Chernyshov, I. Y.; Li, G.; Gascon, J.; Pidko, E. A., Breaking Linear Scaling Relationships with Secondary Interactions in Confined Space: A Case Study of Methane Oxidation by Fe/ZSM-5 Zeolite. *ACS Catal.* **2019,** *9* (10), 9276-9284.
248. Vitillo, J. G.; Lu, C. C.; Cramer, C. J.; Bhan, A.; Gagliardi, L., Influence of First and Second Coordination Environment on Structural Fe(II) Sites in MIL-101 for C–H Bond Activation in Methane. *ACS Catal.* **2020,** *11* (2), 579-589.
249. Sours, T.; Patel, A.; Nørskov, J.; Siahrostami, S.; Kulkarni, A., Circumventing Scaling Relations in Oxygen Electrochemistry Using Metal–Organic Frameworks. *J. Phys. Chem. Lett.* **2020,** *11* (23), 10029-10036.
250. Wang, Y.-H.; Schneider, P. E.; Goldsmith, Z. K.; Mondal, B.; Hammes-Schiffer, S.; Stahl, S. S., Brønsted Acid Scaling Relationships Enable Control Over Product Selectivity from O2 Reduction with a Mononuclear Cobalt Porphyrin Catalyst. *ACS Cent. Sci.* **2019,** *5* (6), 1024-1034.
251. Janesko, B. G.; Scuseria, G. E., Hartree-Fock Orbitals Significantly Improve the Reaction Barrier Heights Predicted by Semilocal Density Functionals. *J. Chem. Phys.* **2008,** *128* (24), 244112.
252. Gani, T. Z. H.; Kulik, H. J., Unifying Exchange Sensitivity in Transition-Metal Spin-State Ordering and Catalysis through Bond Valence Metrics. *J. Chem. Theory Comput.* **2017,** *13* (11), 5443-5457.
253. Mahler, A.; Janesko, B. G.; Moncho, S.; Brothers, E. N., When Hartree-Fock Exchange Admixture Lowers DFT-Predicted Barrier Heights: Natural Bond Orbital Analyses and Implications for Catalysis. *J. Chem. Phys.* **2018,** *148* (24), 244106.
254. Mahler, A.; Janesko, B. G.; Moncho, S.; Brothers, E. N., Why are GGAs so Accurate for Reaction Kinetics on Surfaces? Systematic Comparison of Hybrid vs. Nonhybrid DFT for Representative Reactions. *J. Chem. Phys.* **2017,** *146* (23), 234103.
255. Xu, Z.; Rossmeisl, J.; Kitchin, J. R., A Linear Response DFT+U Study of Trends in the Oxygen Evolution Activity of Transition Metal Rutile Dioxides. *J. Phys. Chem. C* **2015,** *119* (9), 4827–4833.

256. Man, I. C.; Su, H.-Y.; Calle-Vallejo, F.; Hansen, H. A.; Martínez, J. I.; Inoglu, N. G.; Kitchin, J.; Jaramillo, T. F.; Nørskov, J. K.; Rossmeisl, J., Universality in Oxygen Evolution Electrocatalysis on Oxide Surfaces. *ChemCatChem* **2011,** *3* (7), 1159-1165.
257. Zhao, Q.; Kulik, H. J., Where Does the Density Localize in the Solid State? Divergent Behavior for Hybrids and DFT+U. *J. Chem. Theory Comput.* **2018,** *14* (2), 670-683.
258. Curnan, M. T.; Kitchin, J. R., Investigating the Energetic Ordering of Stable and Metastable $TiO_2$ Polymorphs using DFT+ U and Hybrid Functionals. *J. Phys. Chem. C* **2015,** *119* (36), 21060-21071.
259. Fajin, J. L. C.; Vines, F.; Cordeiro, M. N. D. S.; Illas, F.; Gomes, J. R. B., Effect of the Exchange-Correlation Potential on the Transferability of Bronsted-Evans-Polanyi Relationships in Heterogeneous Catalysis. *J. Chem. Theory Comput.* **2016,** *12* (5), 2121-2126.
260. Christensen, R.; Hansen, H. A.; Dickens, C. F.; Nørskov, J. K.; Vegge, T., Functional Independent Scaling Relation for ORR/OER Catalysts. *J. Phys. Chem. C* **2016,** *120* (43), 24910-24916.
261. Cohen, A. J.; Mori-Sanchez, P.; Yang, W., Fractional Charge Perspective on the Band Gap in Density-Functional Theory. *Phys. Rev. B* **2008,** *77* (11), 115123.
262. Cohen, A. J.; Mori-Sanchez, P.; Yang, W., Insights into Current Limitations of Density Functional Theory. *Science* **2008,** *321* (5890), 792-794.
263. Chen, H.; Lai, W.; Shaik, S., Exchange-Enhanced H-Abstraction Reactivity of High-Valent Nonheme Iron(IV)-Oxo from Coupled Cluster and Density Functional Theories. *J. Phys. Chem. Lett.* **2010,** *1* (10), 1533-1540.
264. Feldt, M.; Mata, R. A., Hybrid Local Molecular Orbital: Molecular Orbital Calculations for Open Shell Systems. *J. Chem. Theory Comput.* **2018,** *14* (10), 5192-5202.
265. Feldt, M.; Martin-Fernandez, C.; Harvey, J. N., Energetics of Non-Heme Iron Reactivity: Can *Ab Initio* Calculations Provide the Right Answer? *Phys. Chem. Chem. Phys.* **2020,** *22* (41), 23908-23919.
266. Werner, H.-J.; Schütz, M., An Efficient Local Coupled Cluster Method for Accurate Thermochemistry of Large Systems. *J. Chem. Phys.* **2011,** *135* (14), 144116.
267. Feldt, M.; Phung, Q. M.; Pierloot, K.; Mata, R. A.; Harvey, J. N., Limits of Coupled-Cluster Calculations for Non-Heme Iron Complexes. *J. Chem. Theory Comput.* **2019,** *15* (2), 922-937.
268. Phung, Q. M.; Martin-Fernandez, C.; Harvey, J. N.; Feldt, M., Ab Initio Calculations for Spin-Gaps of Non-Herne Iron Complexes. *J. Chem. Theory Comput.* **2019,** *15* (8), 4297-4304.
269. Hirao, H.; Kumar, D.; Que, L., Jr.; Shaik, S., Two-State Reactivity in Alkane Hydroxylation by Non-Heme Iron-Oxo Complexes. *J. Am. Chem. Soc.* **2006,** *128* (26), 8590-8606.
270. Shaik, S.; Danovich, D.; Fiedler, A.; Schroder, D.; Schwarz, H., 2-State Reactivity in Organometallic Gas-Phase Ion Chemistry. *Helv. Chim. Acta* **1995,** *78* (6), 1393-1407.
271. Pierloot, K.; Phung, Q. M.; Domingo, A., Spin State Energetics in First-Row Transition Metal Complexes: Contribution of (3s3p) Correlation and Its Description by Second-Order Perturbation Theory. *J. Chem. Theory Comput.* **2017,** *13* (2), 537-553.
272. Phung, Q. M.; Feldt, M.; Harvey, J. N.; Pierloot, K., Toward Highly Accurate Spin State Energetics in First-Row Transition Metal Complexes: A Combined CASPT2/CC Approach. *J. Chem. Theory Comput.* **2018,** *14* (5), 2446-2455.
273. Iyer, A. H.; Krishna Deepak, R. N. V.; Sankararamakrishnan, R., Imidazole Nitrogens of Two Histidine Residues Participating in N–H···N Hydrogen Bonds in Protein Structures:

Structural Bioinformatics Approach Combined with Quantum Chemical Calculations. *J. Phys. Chem. B* **2018,** *122* (3), 1205-1212.
274. Yesselman, J. D.; Horowitz, S.; Brooks, C. L.; Trievel, R. C., Frequent Side Chain Methyl Carbon-Oxygen Hydrogen Bonding in Proteins Revealed by Computational and Stereochemical Analysis of Neutron Structures. *Proteins: Structure, Function, and Bioinformatics* **2014,** *83* (3), 403-410.
275. Coulson, C. A.; Danielsson, U., Ionic and Covalent Contributions to the Hydrogen Bond .2. *Ark. Fys.* **1954,** *8* (3), 245-255.
276. Shahi, A.; Arunan, E., Why are Hydrogen Bonds Directional? *J. Chem. Sci.* **2016,** *128* (10), 1571-1577.
277. Cleland, W.; Kreevoy, M., Low-Barrier Hydrogen Bonds and Enzymic Catalysis. *Science* **1994,** *264* (5167), 1887-1890.
278. Vennelakanti, V.; Qi, H. W.; Mehmood, R.; Kulik, H. J., When are Two Hydrogen Bonds Better than One? Accurate First-Principles Models Explain the Balance of Hydrogen Bond Donors and Acceptors Found in Proteins. *Chem. Sci.* **2021,** *12* (3), 1147-1162.
279. Qi, H. W.; Kulik, H. J., Evaluating Unexpectedly Short Non-covalent Distances in X-ray Crystal Structures of Proteins with Electronic Structure Analysis. *J. Chem. Inf. Model.* **2019,** *59* (5), 2199-2211.
280. Jiang, Z.; Biczysko, M.; Moriarty, N. W., Accurate Geometries for "Mountain Pass" Regions of the Ramachandran Plot Using Quantum Chemical Calculations. *Proteins: Structure, Function, and Bioinformatics* **2018,** *86* (3), 273-278.
281. Riniker, S., Fixed-Charge Atomistic Force Fields for Molecular Dynamics Simulations in the Condensed Phase: An Overview. *J. Chem. Inf. Model.* **2018,** *58* (3), 565-578.
282. Boese, A. D., Density Functional Theory and Hydrogen Bonds: Are We There Yet? *ChemPhysChem* **2015,** *16* (5), 978-985.
283. Kristyan, S.; Pulay, P., Can (Semi)Local Density-Functional Theory Account for the London Dispersion Forces. *Chem. Phys. Lett.* **1994,** *229* (3), 175-180.
284. Meijer, E. J.; Sprik, M., A Density-Functional Study of the Intermolecular Interactions of Benzene. *J. Chem. Phys.* **1996,** *105* (19), 8684-8689.
285. Zhou, S.; Wang, L., Unraveling the Structural and Chemical Features of Biological Short Hydrogen Bonds. *Chem. Sci.* **2019,** *10* (33), 7734-7745.
286. Kumar, K.; Woo, S. M.; Siu, T.; Cortopassi, W. A.; Duarte, F.; Paton, R. S., Cation-Pi Interactions in Protein-Ligand Binding: Theory and Data-Mining Reveal Different Roles for Lysine and Arginine. *Chem. Sci.* **2018,** *9* (10), 2655-2665.
287. Hill, E. A.; Weitz, A. C.; Onderko, E.; Romero-Rivera, A.; Guo, Y. S.; Swart, M.; Bominaar, E. L.; Green, M. T.; Hendrich, M. P.; Lacy, D. C.; Borovik, A. S., Reactivity of an Fe-IV-Oxo Complex with Protons and Oxidants. *J. Am. Chem. Soc.* **2016,** *138* (40), 13143-13146.
288. Borovik, A. S., Bioinspired Hydrogen Bond Motifs in Ligand Design: The Role of Noncovalent Interactions in Metal ion Mediated Activation of Dioxygen. *Acc. Chem. Res.* **2005,** *38* (1), 54-61.
289. Oswald, V. F.; Lee, J. L.; Biswas, S.; Weitz, A. C.; Mittra, K.; Fan, R.; Li, J.; Zhao, J.; Hu, M. Y.; Alp, E. E.; Bominaar, E. L.; Guo, Y.; Green, M. T.; Hendrich, M. P.; Borovik, A. S., Effects of Noncovalent Interactions on High-Spin Fe(IV)-Oxido Complexes. *J. Am. Chem. Soc.* **2020,** *142* (27), 11804-11817.

290. Nandy, A.; Duan, C.; Kulik, H. J., Audacity of Huge: Overcoming Challenges of Data Scarcity and Data Quality for Machine Learning in Computational Materials Discovery. *Curr. Opin. in Chem. Eng.* **2022,** *36*, 100778.
291. Kitchin, J. R., Machine Learning in Catalysis. *Nat. Catal.* **2018,** *1* (4), 230-232.
292. Toyao, T.; Maeno, Z.; Takakusagi, S.; Kamachi, T.; Takigawa, I.; Shimizu, K.-i., Machine Learning for Catalysis Informatics: Recent Applications and Prospects. *ACS Catal.* **2019,** *10* (3), 2260-2297.
293. Esterhuizen, J. A.; Goldsmith, B. R.; Linic, S., Interpretable Machine Learning for Knowledge Generation in Heterogeneous Catalysis. *Nat. Catal.* **2022,** *5* (3), 175-184.
294. Meyer, B.; Sawatlon, B.; Heinen, S.; von Lilienfeld, O. A.; Corminboeuf, C., Machine Learning Meets Volcano Plots: Computational Discovery of Cross-Coupling Catalysts. *Chem. Sci.* **2018,** *9* (35), 7069-7077.
295. Wodrich, M. D.; Fabrizio, A.; Meyer, B.; Corminboeuf, C., Data-Powered Augmented Volcano Plots for Homogeneous Catalysis. *Chem. Sci.* **2020,** *11* (44), 12070-12080.
296. Janet, J. P.; Ramesh, S.; Duan, C.; Kulik, H. J., Accurate Multiobjective Design in a Space of Millions of Transition Metal Complexes with Neural-Network-Driven Efficient Global Optimization. *ACS Cent. Sci.* **2020,** *6* (4), 513-524.
297. dos Passos Gomes, G.; Pollice, R.; Aspuru-Guzik, A., Navigating through the Maze of Homogeneous Catalyst Design with Machine Learning. *Trends in Chemistry* **2021,** *3* (2), 96-110.
298. Duan, C.; Liu, F.; Nandy, A.; Kulik, H. J., Putting Density Functional Theory to the Test in Machine-Learning-Accelerated Materials Discovery. *J. Phys. Chem. Lett.* **2021,** *12* (19), 4628-4637.
299. Duan, C.; Nandy, A.; Adamji, H.; Román-Leshkov, Y.; Kulik, H. J., Machine Learning Models Predict Calculation Outcomes with the Transferability Necessary for Computational Catalysis. *J. Chem. Theory Comput.* **2022**, accepted.
300. Chen, S.; Nielson, T.; Zalit, E.; Skjelstad, B. B.; Borough, B.; Hirschi, W. J.; Yu, S.; Balcells, D.; Ess, D. H., Automated Construction and Optimization Combined with Machine Learning to Generate Pt(II) Methane C–H Activation Transition States. *Top. Catal.* **2021,** *65* (1-4), 312-324.
301. Nandy, A.; Duan, C.; Taylor, M. G.; Liu, F.; Steeves, A. H.; Kulik, H. J., Computational Discovery of Transition-metal Complexes: From High-throughput Screening to Machine Learning. *Chem. Rev.* **2021,** *121* (16), 9927-10000.
302. Jablonka, K. M.; Ongari, D.; Moosavi, S. M.; Smit, B., Big-Data Science in Porous Materials: Materials Genomics and Machine Learning. *Chem. Rev.* **2020,** *120* (16), 8066-8129.
303. Rosen, A. S.; Notestein, J. M.; Snurr, R. Q., Realizing the Data-Driven, Computational Discovery of Metal-Organic Framework Catalysts. *Curr. Opin. in Chem. Eng.* **2022,** *35*, 100760.
304. Jablonka, K. M.; Ongari, D.; Moosavi, S. M.; Smit, B., Using Collective Knowledge to Assign Oxidation States of Metal Cations in Metal–Organic Frameworks. *Nat. Chem.* **2021,** *13* (8), 771-777.

**For Table of Contents Use Only**